RE: A point-to-point response to reviewers' comments

"Secondary OH reactions of aromatics-derived oxygenated organic molecules lead to plentiful highly oxygenated organic molecules within an intraday OH exposure" by Yuwei Wang, Yueyang Li, Gan Yang, Xueyan Yang, Yizhen Wu, Chuang Li, Lei Yao, Hefeng, Zhang, Lin Wang (egusphere-2023-1702)

Dear Dr. Liggio,

We are very grateful to the helpful comments from the reviewers, and have carefully revised our manuscript accordingly. A point-to-point response to the comments, which are repeated in *italic*, is given below.

We are looking forward to your decision at your earliest convenience.

Best regards,

Lin Wang
Fudan University
lin_wang@fudan.edu.cn

Reviewer #1

Significance

Aromatic compound oxidation is responsible for a sizeable fraction of urban air pollution. Aromatics contribute significantly to the condensable product pool, and consequently are an important source, often even the dominant, of anthropogenic secondary organic aerosol (SOA). The autoxidation pathways to highly oxygenated organic compounds (HOM) from aromatics have puzzled the atmospheric community for around a decade and the major achievements on the topic have been published in several previous works (e.g., Wang et al., 2017, Molteni et al., 2018, Garmash et al., 2020 etc.). The current work aims to add to this by studying 1,3,5-trimethylbenzene (mesitylene) in an oxidation flow reactor setup using far above ambient OH concentrations, attempting to simulate long atmospheric oxidation timescales.

While the research performed is certainly timely, it has been performed with methodology that unrealistically biases the oxidation conditions, and thus prevents gaining the sought after mechanistic insight. While the used oxidation flow reactor approach has its merits in developing emission regulations, it is not a platform for studying detailed molecular level oxidation chemistry of atmospheric relevant condensable product formation. As such, I can only recommend rejecting the work with its current analysis and conclusions. Below I detail why I feel the work is performed with inadequate research methodology, and I'll point out several issues I hope the authors will pay attention in preparing the next draft for submission.

Response:

We are very sorry that Reviewer #1 was concerned about the experimental setup in this study, which in fact has been practiced and evaluated, in addition to by three studies that have been cited by Reviewer #1 himself several lines above (*Wang et al., 2017, Molteni et al., 2018, Garmash et al., 2020*), in a number of previous studies (e.g., Tsiligiannis et al., 2019; Cheng et al., 2021). Below we will address his concerns in details, and try to convince Reviewer #1 that results in the current methodology are applicable to oxidation mechanisms.

Major comments

Q 1.1 *Unfortunately, the PAM OFR setup used in the current work with very high [OH] is not suitable for studying mechanistic details of atmospheric oxidation, perhaps even less of aromatic compound oxidation where the sequential OH oxidation and photo-oxidation of intermediates and products is important. The PAM methodology has been constructed to allow estimating the potential aerosol mass from a given emission, and it is really a method aiming for emission regulations, rather than molecular level mechanistic details. The high OH concentrations lead to unrealistically high primary radical concentrations and skew the reaction system towards very rapid RO_2 + OH pathways. The design also necessarily leads into higher RO_2 + RO_2 rates favoring accretion product formation, but also radical propagation channels by RO formation. Additionally, the formation rate of closed-shell species is accelerated allowing for more efficient sequential OH oxidation. According to the presented results, even oxidation of the accretion products is possible that commonly would be expected to contribute to the growing aerosol, and not be lost in chemical degradation by reactions with oxidants. In the atmosphere it really matters what is the correct reaction timescale, and thus the order of the sequential reactions. Hence, it's difficult to see how a PAM type setup could be used to study mechanistic details of atmospheric oxidation chains .*

So, once again, PAM was constructed to enable making emission regulations, and not for studying

details of atmospheric chemistry, though several groups have seemed to adopt it for such a purpose recently. PAM is by design non-linear in oxidation chemistry regime and is thus not capable for detailing the molecular mechanisms. As the Authors also confess, the autoxidation pathways are the most important at low loadings, when processes like RO_2 + RO_2, and RO_2 + OH, are suppressed. The timing and order of reactions happening in a sequential oxidation do make a big impact.

Response 1.1:

We are very grateful for comments on our manuscript by Reviewer #1.

As stated in the manuscript, the current OH does settings were deliberately selected. Following the definition by Garmash et al. (2020), OH concentrations integrated over the corresponding residence time would define an OH dose, which is also referred as OH exposure and can be used to compare results between different systems or to those in the ambient atmosphere. We set our OH concentration as used in our experiments in order to obtain a desired OH dose, i.e., an intraday OH exposure, which fills the current gap in terms of the extent of oxidation of aromatics in previous studies that focused on HOMs. Garmash et al. (2020) and Cheng et al. (2021) both used an extremely high OH exposure, which is equivalent to atmospheric oxidation times of 6.7 hours - 10 days and 2.4 - 19.4 days at OH concentrations of 1.5×10^6 molecule cm^{-3}, respectively. OH exposures in our experiments, on the other hand, are roughly equivalent to atmospheric oxidation times of 0.9 – 9.2 hours at OH concentrations of 1.5×10^6 molecule cm^{-3}.

Also, to avoid potential misunderstanding, we would like to note that though we used a PAM OFR to conduct our experiments, our settings were much different from the traditional settings of PAM utilized in previous investigations (e.g., Kang et al., 2007). In the traditional settings of PAM, a large OH exposure equivalent to ~ 10 days was utilized to generate amounts of aerosols to investigate potential aerosols formed by given precursors. In this study, we merely used the hardware of PAM and actually used PAM as an OFR with relatively low OH exposures.

Indeed, the main concerns raised by Reviewer #1 that important processes in OFR, i.e., photolysis, RO_2 isomerization, and condensation, may do not scale with OH equally, are important issues. To validate our settings, a PAM chemistry model (PAM_chem_v8), utilized widely in previous studies, is chosen with the latest updates to calculate radical profiles in our OFR (Li et al., 2015; Cheng et al., 2021; Wang et al., 2020; Mehra et al., 2020; Lambe et al., 2015, 2018; Peng and Jimenez, 2020; Lambe et al., 2017). This model is based on a photochemical box model that includes chemistry of photolysis of oxygen, water vapor, and other trace gases by the primary wavelengths of mercury lamps, and simplified VOC and RO_2 chemistry, but further reactions of the first-generation stabilized products and the second-generation organic radicals are not considered (Table R1, also as Table S2 in the revised manuscript). Kinetic data for this modified PAM chemistry model are obtained from the IUPAC (International Union of Pure and Applied Chemistry) dataset (https://iupac-aeris.ipsl.fr, last access: 26 October 2023) and the MCM dataset (MCM v3.3.1, https://mcm.york.ac.uk/MCM/, last access: 9 October 2023), except for those that are specifically discussed in details below. Note that the total RO_2 concentration is simplified to be the sum of concentrations of BPR and $C_9H_{13}O_7$· in our study.

Table R1. Reactions included in the modified PAM_chem_v8 under the settings with only 254 nm UV lights on. For experiments in the absence of NO_x, the input value of N_2O is 0 and all the NO_x-related reactions proceed with a zero rate. RO_2 is the sum of BPR and $C_9H_{13}O_7$· for simplification.

No	Reactions	Reaction rate constants/photolysis rate

		(molecule^{-1} cm^3 s^{-1}/ s^{-1})
1	$HO_2 + h\nu$ (λ = 254 nm) = $OH + O(^1D)$	$2.63\times10^{-19}\times flux_{254}$
2	$O_3 + O(^1D) = 2O_2$	1.20×10^{-10}
3	$O_3 + O(^1D) = O + O + O_2$	1.20×10^{-10}
4	$O + OH = H + O_2$	$2.20\times10^{-11}\times e^{120/T}$
5	$O(^1D) + H_2 = OH + H$	1.20×10^{-10}
6	$HO_2 + H = 2OH$	7.20×10^{-11}
7	$HO_2 + H = O + H_2O$	1.60×10^{-12}
8	$HO_2 + H = H_2 + O_2$	6.90×10^{-12}
9	$O_3 + H = OH + O_2$	$1.40\times10^{-11}\times e^{-470/T}$
10	$N_2O + O(^1D) = 2NO$	$6.70\times10^{-11}\times e^{20/T}$
11	$N_2O + O(^1D) = N_2 + O_2$	$4.70\times10^{-11}\times e^{20/T}$
12	$O + HO_2 = OH + O_2$	$3.02\times10^{-11}\times e^{200/T}$
13	$O + H_2O_2 = OH + HO_2$	$1.40\times10^{-12}\times e^{-2000/T}$
14	$O + O_3 = 2O_2$	$8.00\times10^{-12}\times e^{-2060/T}$
15	$O + NO_3 = NO_2 + O_2$	1.00×10^{-11}
16	$O + NO_2 = NO + O_2$	$5.12\times10^{-12}\times e^{210/T}$
17	$OH + O_3 = HO_2 + O_2$	$1.70\times10^{-12}\times e^{-940/T}$
18	$OH + HO_2 = H_2O + O_2$	$4.80\times10^{-11}\times e^{250/T}$
19	$OH + HONO = H_2O + NO_2$	$1.80\times10^{-11}\times e^{-390/T}$
20	$OH + H_2O_2 = H_2O + HO_2$	$2.90\times10^{-12}\times e^{-160/T}$
21	$OH + H_2 = H_2O + H$	$2.80\times10^{-12}\times e^{-1800/T}$
22	$OH + OH = H_2O + O$	1.80×10^{-12}
23	$HO_2 + O_3 = OH + O_2$	$1.00\times10^{-14}\times e^{-490/T}$
24	$HO_2 + NO = OH + NO_2$	$3.50\times10^{-12}\times e^{270/T}$
25	$NO + O_3 = NO_2 + O_2$	$2.00\times10^{-12}\times e^{-1400/T}$
26	$NO_2 + O_3 = NO_3 + O_2$	$1.20\times10^{-13}\times e^{-2450/T}$
27	$NO + NO_3 = 2NO + O_2$	$1.50\times10^{-11}\times e^{170/T}$
28	$NO_3 + NO_3 = 2NO_2 + O_2$	$8.50\times10^{-13}\times e^{-2450/T}$
29	$N_2O_5 + H_2O = 2HNO_3$	2.00×10^{-21}
30	$O + O_2 + M = O_3 + M$	$6.00\times10^{-34}\times M\times(300/T)^{2.4}$
31	$H + O_2 + M = HO_2 + M$	$k_o = 4.40\times10^{-32}\times M\times(300/T)^{1.3}$ $k_h = 7.50\times10^{-11}\times(300/T)^{0.2}$ $k = k_o/(1+(k_o/k_h))\times0.6^{(1+(\log10(k_o/k_h))^{-2}}$
32	$OH + OH + M = H_2O_2 + M$	$k_o = 6.90\times10^{-31}\times M\times(300/T)$ $k_h = 2.60\times10^{-11}$ $k = k_o/(1+(k_o/k_h))\times0.6^{(1+(\log10(k_o/k_h))^{-2}}$
33	$OH + NO + M = HONO + M$	$k_o = 7.00\times10^{-31}\times M\times(300/T)^{2.6}$ $k_h = 3.60\times10^{-11}\times(300/T)^{0.1}$ $k = k_o/(1+(k_o/k_h))\times0.6^{(1+(\log10(k_o/k_h))^{-2}}$
34	$OH + NO_2 + M = HNO_3 + M$	$k_o = 1.80\times10^{-30}\times M\times(300/T)^{2.6}$ $k_h = 2.80\times10^{-11}$ $k = k_o/(1+(k_o/k_h))\times0.6^{(1+(\log10(k_o/k_h))^{-2}}$
35	$OH + HNO_3 = H_2O + NO_3$	$k_{00} = 2.40\times10^{-14}\times e^{460/T}$ $k_{01} = 6.50\times10^{-34}\times e^{2199/T}$ $k_{02} = 2.80\times10^{-11}\times e^{-2450/T}$ $k = k_{00} + (k_{01}\times M)/(1+(k_{01}\times M)/k_{02})$
36	$HO_2 + NO_2 + M = HO_2NO_2 + M$	$k_o = 1.80\times10^{-31}\times M\times(300/T)^{3.2}$ $k_h = 4.70\times10^{-12}\times(300/T)^{1.4}$ $k = k_o/(1+(k_o/k_h))\times0.6^{(1+(\log10(k_o/k_h))^{-2}}$ $k_{reverse} = k/(2.10\times10^{-27}\times e^{10900/T})$
37	$NO_2 + NO_3 + M = N_2O_5 + M$	$k_o = 2.00\times10^{-30}\times M\times(300/T)^{4.4}$ $k_h = 1.40\times10^{-12}\times(300/T)^{0.7}$ $k = k_o/(1+(k_o/k_h))\times0.6^{(1+(\log10(k_o/k_h))^{-2}}$ $k_{reverse} = k/(2.70\times10^{-27}\times e^{11000/T})$

38	OH + HNO_4 = products	$1.30\times10^{-12}\times e^{250/T}$
39	Sci + H_2O = products	4.00×10^{-15}
40	1,3,5-TMB + OH = BPR	$0.8\times5.67\times10^{-11}$
41	1,3,5-TMB + OH = Products	$0.2\times5.67\times10^{-11}$
42	BPR = C9H13O7	7
43	BPR + RO_2 = ROOR'	1.70×10^{-10}
44	BPR + RO_2 = R=O/ROH + O_2	$0.4\times8.8\times10^{-13}$
45	BPR + RO_2 = 2RO + O_2	$0.6\times8.8\times10^{-13}$
46	BPR + OH = RPO_2 + H_2O	1.00×10^{-10}
47	BPR + HO_2 = ROOH + O_2	1.20×10^{-11}
48	BPR = wall loss	0.0023
49	BPR + NO = RO + NO_2	$0.843\times8.50\times10^{-12}$
50	BPR + NO + M = $RONO_2$+ M	$0.157\times8.50\times10^{-12}$
51	C9H13O7 + RO_2 = ROOR'	2.60×10^{-10}
52	C9H13O7 + RO_2 = R=O/ROH + O_2	$0.4\times8.8\times10^{-13}$
53	C9H13O7 + RO_2 = 2RO + O_2	$0.6\times8.8\times10^{-13}$
54	C9H13O7 + OH = RPO_2 + H_2O	1.00×10^{-10}
55	C9H13O7 + HO_2 = ROOH + O_2	1.20×10^{-11}
56	C9H13O7 = wall loss	0.0023
57	C9H13O7+ NO = RO + NO_2	$0.843\times8.50\times10^{-12}$
58	C9H13O7 + NO + M = $RONO_2$+ M	$0.157\times8.50\times10^{-12}$
59	ROOH + OH = RO_2 + H_2O	$5.30\times10^{-12}\times e^{190/T}\times0.6$
60	ROOH + OH = RPHO + OH + H_2O	$5.30\times10^{-12}\times e^{190/T}\times0.4$
61	RO + O_2 = RPO + HO_2	6.00×10^{-15}
62	H_2O_2 + *hv* (λ = 254 nm) = 2OH	$6.70\times10^{-20}\times flux_{254}$
63	NO_2 + *hv* (λ = 254 nm) = O + NO	$1.00\times10^{-20}\times flux_{254}$
64	HONO + *hv* (λ = 254 nm) = OH + NO	$1.40\times10^{-19}\times flux_{254}$
65	HNO_3 + *hv* (λ = 254 nm) = OH + NO_2	$1.95\times10^{-20}\times flux_{254}$
66	HNO_4 + *hv* (λ = 254 nm) = HO_2 + NO_2	$3.60\times10^{-19}\times flux_{254}$
67	N_2O_5 + *hv* (λ = 254 nm) = NO_2 + NO_3	$3.20\times10^{-19}\times flux_{254}$

In this work, autoxidation and accretion of 1,3,5-TMB-derived BPR, as well as the subsequent reactions of the autoxidation product of BPR, i.e., $C_9H_{13}O_7$·, are newly implemented or modified in this model (Reaction No. 42 – 58 in Table R1). The pathways of peroxy radicals and their kinetics are discussed below. NO_x-related reactions are also included in the model. When we simulate experiments without NO_x, these reactions do not contribute to the simulation results.

RO_2 can react with a number of radicals, generating termination products or other radicals.

$$RO_2 + R'O_2 \rightarrow RO + R'O + O_2 \quad (R1)$$

$$RO_2 + R'O_2 \rightarrow R=O + R'OH + O_2 \quad (R2)$$

$$RO_2 + R'O_2 \rightarrow ROH + R'=O + O_2 \quad (R3)$$

$$RO_2 + R'O_2 \rightarrow ROOR' + O_2 \quad (R4)$$

$$RO_2 + HO_2 \rightarrow ROOH + O_2 \quad (R5)$$

$R1$, $R2$, and $R3$ are reactions of RO_2 + RO_2, forming alkoxy radicals, carbonyl termination products, and hydroxyl termination products, respectively. $R4$ is an accretion reaction, forming dimers via combination of two monomeric RO_2. $R5$ is the reaction between RO_2 and HO_2, forming hydroperoxyl radicals. The reaction rate constants for RO_2 in $R1$ – $R5$ are obtained by MCM or previous investigations (e.g., Jenkin et al., 2003; Berndt et al., 2018; Peng and Jimenez, 2020). We treat $R1$ – $R3$ as a total reaction with a reaction rate constant of 8.8×10^{-13} molecule^{-1} cm^3 s^{-1}, and branching ratios of $R1 - R3$ of 0.6, 0.2, and 0.2, respectively, as suggested by MCM (Jenkin et al., 2003). The reaction rate constants of BPR and $C_9H_{13}O_7$· for $R4$ are 1.7×10^{-10} and 2.6×10^{-10} molecule^{-1} cm^3 s^{-1}, respectively (Berndt et al., 2018). The reaction rate constants for $R5$ is $1.5\times10^{-}$

^{11} molecule^{-1} cm^3 s^{-1} (Jenkin et al., 2003).

$$RO_2 + OH \rightarrow Products \qquad (R6)$$

$R6$ is the reaction between OH and RO_2. The reaction rate constant for $R6$ is 1×10^{-10} molecule^{-1} cm^3 s^{-1} according to previous studies (Bossolasco et al., 2014; Yan et al., 2016; Assaf et al., 2016, 2017; Peng and Jimenez, 2020). Current knowledge on the reaction products for the reaction of $CH_3O_2\cdot$ + OH, the most studied RO_2 + OH reaction, is summarized in Table R2 (also as Table S3). The products of this reaction are suggested to include a Criegee intermediate ($CH_2O_2\cdot$), a stabilized methylhydrotrioxide (CH_3OOOH), an alkoxy radical ($CH_3O\cdot$), and methanol (CH_3OH) (Yan et al., 2016; Fittschen, 2019; Caravan et al., 2018; Müller et al., 2016). Müller et al. (2016) and Caravan et al. (2018) suggest that the formation of $CH_2O_2\cdot$ is actually infeasible, and Yan et al. (2016) estimated an upper limit branching ratio of 5% for this pathway. The branching ratios of stabilized products CH_3OH and CH_3OOOH are 6 - 7% (Caravan et al., 2018; Müller et al., 2016) and 7% (Müller et al., 2016), respectively. The most significant product of this reaction is the alkoxy radical ($CH_3O\cdot$), with a branching ratio of more than 86% (Müller et al., 2016). In the absence of NO_x, CH_3OH and $CH_3O\cdot$ can also be formed via the traditional unimolecular reaction between $CH_3O_2\cdot$ and RO_2, i.e., $R1$ and $R3$. The possible role of this reaction of large RO_2, i.e., BPR and other C9-RO_2, with OH has not yet been investigated. However, according to the branching ratios for the reaction of $CH_3O_2\cdot$ + OH, this reaction is likely to form RO instead of stabilized C9 products. Hence, we assume that the branching ratios of hydrotrioxide (ROOOH), RO, and ROH are 0.07, 0.86, and 0.07, respectively, for BPR + OH and C9-RO_2 + OH.

Table R2. The branching ratios of different pathways for $CH_3O_2\cdot$ + OH.

Reactions	Branching ratio	References
$CH_3O_2\cdot + OH \rightarrow CH_2O_2\cdot + H_2O$	< 5%	(Yan et al., 2016)
	0	(Caravan et al., 2018; Müller et al., 2016)
$CH_3O_2\cdot + OH \rightarrow CH_3O\cdot + HO_2$	86%	(Müller et al., 2016)
$CH_3O_2\cdot + OH \rightarrow CH_3OH + HO_2$	6 ± 2%	(Caravan et al., 2018)
	7%	(Müller et al., 2016)
$CH_3O_2\cdot + OH \rightarrow CH_3OOOH$	7%	(Müller et al., 2016)

$$RO_2 \xrightarrow{isomerization} Products \qquad (R7)$$

Unimolecular reactions can also contribute to consumption of RO_2 in the PAM OFR. RO_2 isomerization rate coefficients are highly dependent on their structures, spanning from 10^{-3} - 10^6 s^{-1} (Bianchi et al., 2019; Crounse et al., 2013; Knap and Jørgensen, 2017; Praske et al., 2018). However, only some substituted acyl RO_2 can undergo rapid isomerization at a reaction rate of 10^6 s^{-1} (Knap and Jørgensen, 2017). 1,3,5-TMB-derived BPR and its autoxidation product, $C_9H_{13}O_7\cdot$, do not belong to the group of substituted acyl RO_2 (Molteni et al., 2018; Tsiligiannis et al., 2019). The most important unimolecular reactions for 1,3,5-TMB-derived BPR is likely autoxidation while the precise autoxidation reaction rates of 1,3,5-TMB-derived BPR and other RO_2 in this system are currently unclear (Bianchi et al., 2019; Molteni et al., 2018). Previous theoretical investigations suggest that more than 90% BPR generated by the oxidation of 1,3,5-TMB possess a structure favoring autoxidation and thus their overall autoxidation reaction rate is relatively fast (Wang et al., 2017). Laboratory experiments also indicate a higher HOM molar yield for 1,3,5-TMB than

ethylbenzene and xylenes (Molteni et al., 2018). We arbitrarily set the autoxidation reaction rate of 1,3,5-TMB-derived BPR the same as that of ethylbenzene-derived BPR, i.e., 7.0 s^{-1}, as a lower limit to estimate the fate of 1,3,5-TMB-derived RO_2 (Wang et al., 2017). Indeed, this value is not necessarily appropriate for all the RO_2 in this system and this estimation is a simplified result mainly based on the most important RO_2 in the oxidation of 1,3,5-TMB, i.e., BPR. Meanwhile, this value will not influence the total concentration of RO_2 but the concentration of BPR, as the total RO_2 concentration is simplified to be the sum of concentrations of BPR and $C_9H_{13}O_7$·.

The reactions between NO and RO_2 can generate alkoxy radicals similar to $R1$ and organonitrates, which are regarded as $R8$ and $R9$.

$$RO_2 + NO \rightarrow RO + NO_2 \qquad (R8)$$

$$RO_2 + NO \rightarrow RONO_2 \qquad (R9)$$

The reaction rate for the sum of these two reactions is taken as 8.5×10^{-12} $molecule^{-1}$ cm^3 s^{-1}. The branching ratios of these two reactions are 0.843 and 0.157, respectively, according to MCM (Jenkin et al., 2003).

Alkoxy radicals, RO, will be generated in $R1$, $R6$, and $R8$. The widely used near-explicit mechanism, MCM, assumes that RO formed via the alkoxy channel of BPR ($R1$) will decompose into small molecules. Recently, Xu et al. (2020) probed the chemical fates of BPR-derived RO, hereafter referred to as bicyclic alkoxy radical (BCP-oxy), in the oxidation of benzene by laboratory experiments and model calculations, which can be taken as a reference to induce the mechanism of 135-TMB-derived BCP-oxy. BCP-oxy can undergo two reactions, i.e., ring-breakage and ring-closure, and a new calculation result suggests that the branching ratio of ring-breakage reaction is larger than 98% (Wang et al., 2013). 56% of ring-breakage reactions will break benzene-derived BCP-oxy into butenedial and glyoxal, and the rest 44% will generate a C6 alkyl radical by the 1,5-aldehydic H-shift. The latter C6 alkyl radical will further undergo other reactions, including a 93% branching ratio for decomposition reactions that results in a reduction of carbon atom number (Xu et al., 2020). Therefore, most of benzene-derived BCP-oxy will likely decompose into compounds with fewer carbon atoms. We assume that 1,3,5-TMB-derived BCP-oxy will undertake these decomposition reactions with a similar branching ratio, which means that these radicals cannot form a large number of stabilized products that can influence the distributions of stabilized C9 products in nitrate CIMS.

The physical loss of RO_2 in the PAM OFR consists of the condensation loss to the aerosol particles and the diffusion loss to the OFR walls, which can be regarded as $R10$.

$$RO_2 \rightarrow physical\ loss \qquad (R10)$$

In our experiments, measurement results by a long-SMPS show that the aerosol particles presented in the PAM OFR were few and thus the condensation loss of HOMs to the aerosol particles was minor and not further considered. The first-order loss rate of HOMs to the OFR walls, k_{wall}, is limited by eddy diffusion and can be calculated with the following function (Cheng et al., 2021; Palm et al., 2016; McMurry and Grosjean, 1985):

$$k_{wall} = \frac{A}{V} \cdot \frac{2}{\pi} \cdot \sqrt{k_e D_g} \qquad (Eq1)$$

where the OFR surface-area-volume ratio (A/V) is 25 m^{-1} and the coefficient of eddy diffusion (k_e) is 0.0042 s^{-1}, as estimated by the method utilized in a previous study (Brune, 2019) and given in $Eq2$.

$$k_e = 0.004 + 10^{-2.25} V^{0.74} \quad (Eq2)$$

where V is the enclosure volume (m^3). The molecular diffusion coefficient, D_g, is estimated with the method as described by Fuller et al. (1966) and is around 5×10^{-6} m^2 s^{-1} with 1,3,5-TMB derived BPR as an example. Hence, k_{wall} is around 0.0023 s^{-1} in the PAM OFR.

The input parameters of temperature, mean residence time, water vapor concentration, O_3 concentration, and the initial 1,3,5-TMB concentration are 25 °C, 53 s, 0.8%, 500 ppbv, and 50 ppbv, respectively, as measured directly in the experiments. The actinic flux at 254 nm, I_{254}, is constrained by comparing OH exposures by model output and OH exposures estimated by the consumption of 1,3,5-TMB as measured by a Vocus PTR. Consumption of O_3 estimated by the model agrees well with the measured results, with discrepancies being always within 10% at different OH exposures.

The above calculation allows us to evaluate radical concentrations and fates of RO_2 in our OFR, and to compare results between our experiments and those under ambient conditions.

Concentration profiles of OH, RO_2, and HO_2 as a function of OH exposures in our experiments without NO_x are illustrated in Figure R1a (also as Figure S1a). According to the modified PAM_chem_v8, when OH increased from 1.09×10^8 to 1.57×10^9 molecule cm^{-3}, HO_2 concentrations increased from 7.72×10^8 to 3.18×10^9 molecule cm^{-3}, whereas RO_2 concentrations increased from 4.83×10^9 to 8.48×10^9 molecule cm^{-3}. The radical concentrations in our experiments with NO_x (Figure R1b, also as Figure S1b) varied in a similar range, with RO_2 ranging from 3.89×10^9 to 9.34×10^9 molecule cm^{-3}, HO_2 ranging from 3.66×10^9 to 6.82×10^9 molecule cm^{-3}, and OH ranging from 4.83×10^8 to 9.05×10^8 molecule cm^{-3}, respectively. The ratios between HO_2/OH and RO_2/OH in our experiments are displayed in Figure R1c (also as Figure S1c). The HO_2/OH ratio ranged between 1.9 and 7.1 in our PAM OFR experiments without NO_x, and the RO_2/OH ratio ranged between 4.9 and 47.9. In experiments with NO_x, the HO_2/OH ratio ranged between 3.7 and 17.9, whilst the RO_2/OH ratio ranged between 4.0 and 13.2. A recent comprehensive ambient campaign conducted in the wintertime central Beijing reported mean daytime peak concentrations of 8.8×10^7, 3.9×10^7, and 2.7×10^6 molecule cm^{-3} for total RO_2, HO_2, and OH, respectively (Slater et al., 2020), which corresponds to ambient RO_2/OH and HO_2/OH ratios of 32.6 and 14.4 (Figure R1c), respectively. Therefore, radical ratios in our flow tube were generally in the same order of magnitude with the ambient conditions.

(a)

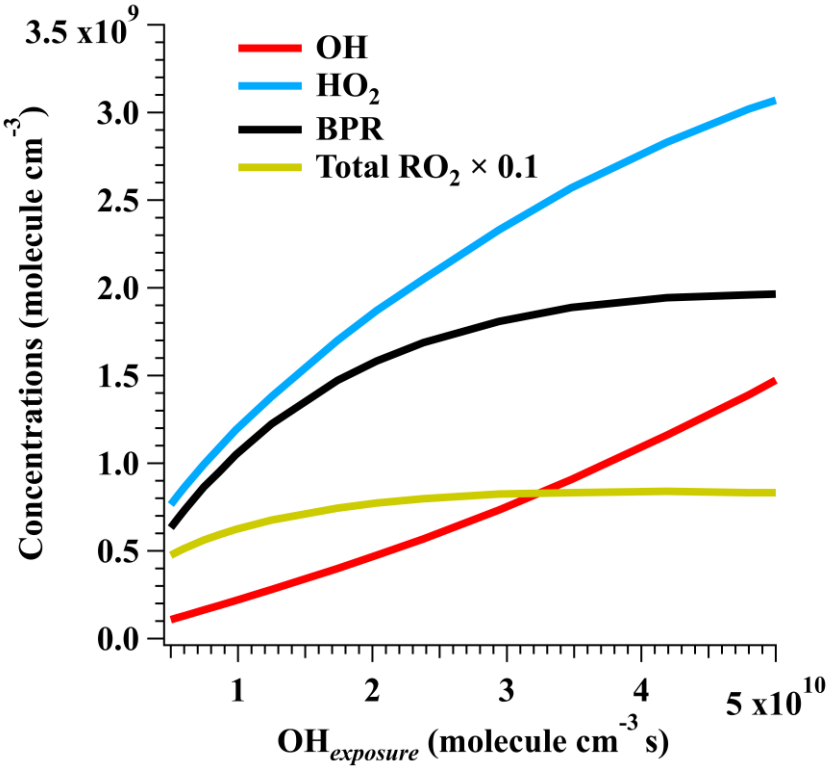
3.5 x10^9
3.0
2.5
2.0
1.5
1.0
0.5
0.0
Concentrations (molecule cm^-3)
OH
HO2
BPR
Total RO2 × 0.1
1
2
3
4
5 x10^10
OHexposure (molecule cm^-3 s)

(b)

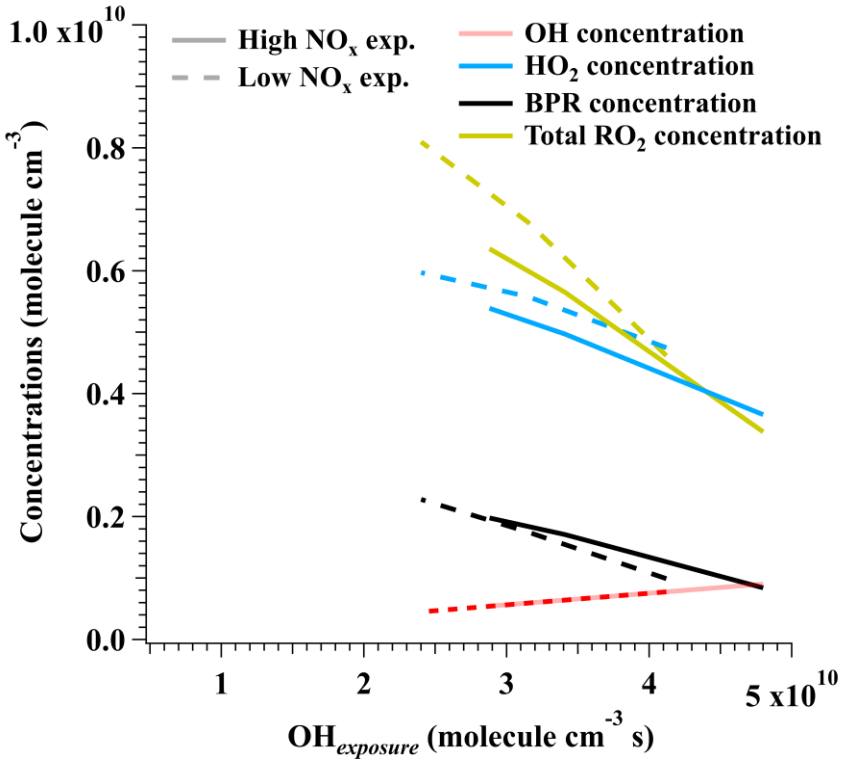
1.0 x10^10
0.8
0.6
0.4
0.2
0.0
Concentrations (molecule cm^-3)
High NOx exp.
Low NOx exp.
OH concentration
HO2 concentration
BPR concentration
Total RO2 concentration
1
2
3
4
5 x10^10
OHexposure (molecule cm^-3 s)

(c)

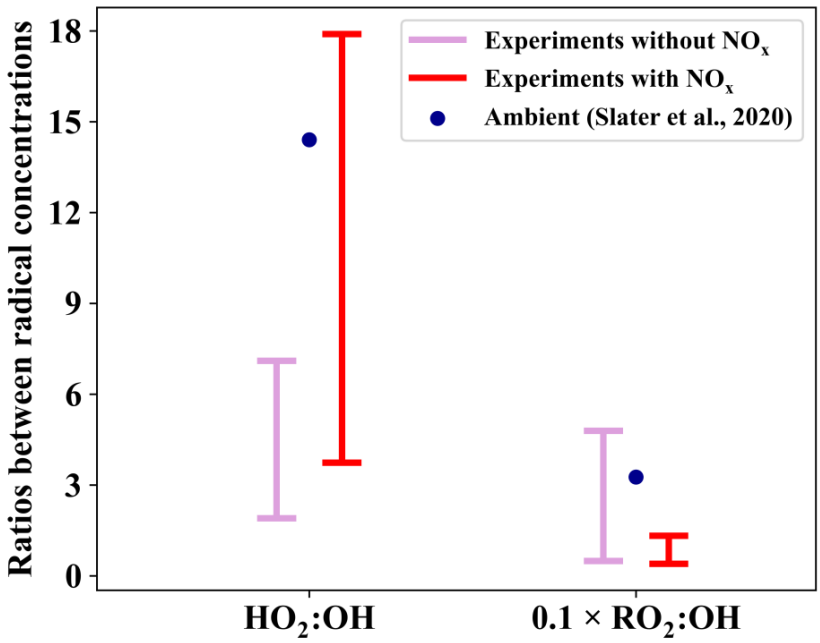

Figure R1. (a) Concentration profiles of OH, HO_2, BPR, and total RO_2 in the PAM OFR experiments without NO_x, as a function of OH exposures. The average total concentrations of RO_2 were scaled with a factor of 0.1 for a better visualization. (b) Concentration profiles of OH, HO_2, BPR, and total RO_2 in the PAM OFR experiments with NO_x, as a function of OH exposures. The average total concentrations of RO_2 were scaled with a factor of 0.1 for a better visualization. (c) HO_2/OH, RO_2×0.1/OH, and their ambient values. The ambient values were calculated according to Slater et al. (2020).

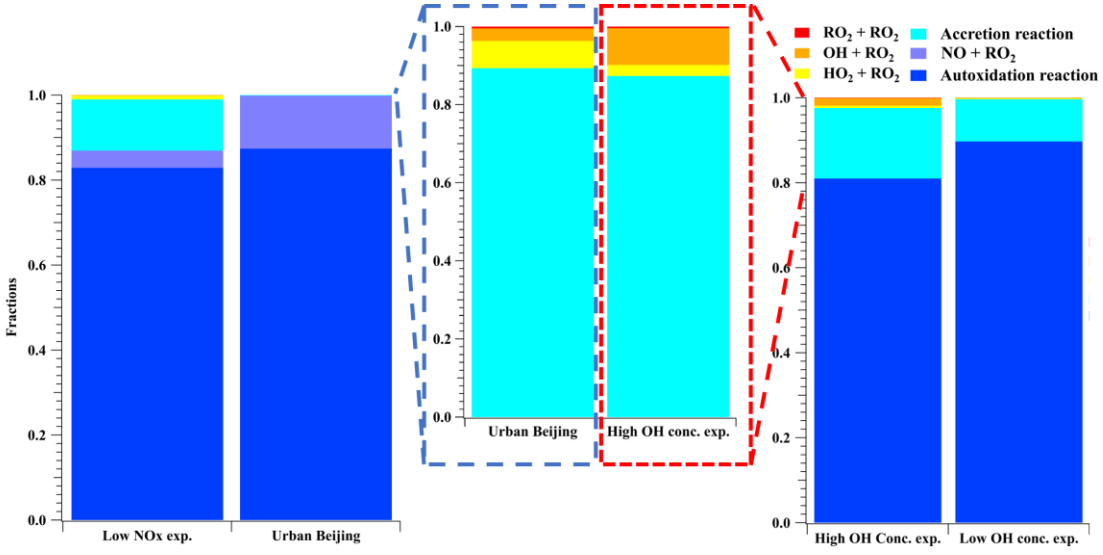

Figure R2. Fates of RO_2 generated in the low NO_x experiment (Exp. 44), urban Beijing (Slater et al., 2020), low OH and zero NO_x experiment (Exp. 19), and high OH and zero NO_x experiment (Exp. 12). Note that RO_2 fates of RO_2, OH, HO_2, and accretion channels are blown up for a better

comparison for urban Beijing and the high OH and zero NO_x experiment. Reactions and kinetic rate coefficients used in the calculations are provided in Table R1.

We take Exp. 12, 19 and 44 as representative examples and compare simulation results with those from the ambient environment (Slater et al., 2020). RO_2 in our experiments mainly consists of RO_2 with multiple oxygenated functionalities and high carbon contents, i.e., BPR and its isomerization products that can undergo accretion reactions as fast as 10^{-10} molecule^{-1} cm^3 s^{-1}. However, only around 50% RO_2 in the real atmosphere are derived from aromatics and long-chain-alkanes containing carbon atoms larger than 4that can undertake accretion reactions at a considerable reaction rate coefficient (Berndt et al., 2018; Bianchi et al., 2019), as observed in Beijing (Slater et al., 2020; Tan et al., 2018). Therefore, the accretion reaction in the ambient is assumed to proceed at half of the accretion reaction rate coefficient of BPR, i.e., 8.5×10^{-11} molecule^{-1} cm^3 s^{-1}.

The RO_2 lifetime in urban Beijing (Slater et al., 2020), low NO_x experiment, low OH and zero NO_x experiment, and high OH and zero NO_x concentration experiment was 1.0, 0.7, 1.2, and 0.6 s, respectively. As shown in Figure R2 (also as Figure 1 in the revised manuscript), In the low NO_x experiment (Exp. 44), the fractions of RO_2 + RO_2 ($R1 - R3$), accretion reaction ($R4$), RO_2 + HO_2 ($R5$), RO_2 + OH ($R6$), autoxidation ($R7$), and RO_2 + NO ($R8 - R9$) were 0.06%, 12.1%, 0.9%, 0.07%, 82.9%, and 4.0%, respectively. Calculated based on the mean daytime peak concentrations of radicals in Beijing (Slater et al., 2020), the fractions of $R1 - R3$, $R4$, $R5$, $R6$, $R7$, and $R8 - R9$ were 0.0005%, 0.09%, 0.007%, 0.003%, 87.4%, and 12.5%, respectively. For the experiment with low OH and zero NO_x (Exp. 19), the fractions of $R1 - R3$, $R4$, $R5$, $R6$, and $R7$ were 0.05%, 10.0%, 0.15%, 0.14%, and 89.7%, respectively. For the one with high OH and zero NO_x (Exp. 12), the fractions of $R1 - R3$, $R4$, $R5$, $R6$, and $R7$ were 0.08%, 16.6%, 0.54%, 1.8%, and 81.0%, respectively. The overall lifetimes of RO_2 and the fractions of autooxidation together determine the significant and similar roles of autoxidation in both laboratory experiments and the ambient. Therefore, the autoxidation chain will run to a similar oxidation level between the laboratory and the ambient.

In experiments in the presence of NO_x (e.g., Exp. 44), though the yields of organonitrates were lower in the laboratory experiments, the formation pathways of these compounds were the same as those in the ambient. Based on the formulae of organonitrates, the detailed formulae for monomer RO_2 could be probed, which helps to investigate the existence of multi-generation OH oxidation. Alkoxy radicals generated in the NO termination channel will unlikely influence the distributions of C9 stabilized products since they tend to get decomposed in the subsequent reactions, as discussed above.

In experiments in absence of NO_x (e.g., Exp. 12 and 19), the proportions of $R8$ - $R9$, i.e., the NO channel in urban environment were reassigned to termination reactions of $R1$ - $R6$, i.e., RO_2 + RO_2, accretion reaction, RO_2 + HO_2, and RO_2 + OH. Comparison of relative fractions of RO_2 fates of RO_2, OH, HO_2, and accretion channels (Figure R2) shows similarities between laboratory and ambient results. By expanding proportions of these termination reactions, laboratory investigations on distributions of products can be facilitated, as the detection of certain HOM products became more precise and the mass spectra became simplified. As discussed in the "results" session, products of $R2$, $R3$, and $R5$ channels of the main BPR were not detected in our experiments due to their low oxygen contents, while secondary products between products of $R2$, $R3$, and $R5$ channels of the

main BPR and OH were observed. Together with stabilized products and secondary products from $C_9H_{13}O_7$· (the peroxy radical formed from autooxidation of BPR), secondary products between products of $R2$, $R3$, and $R5$ channels of the main BPR and OH help to elucidate the first- and multi-generation reaction pathways in the 1,3,5-TMB+OH system, according to their molecular formular.

On the other hand, the much-expanded proportion of HOM dimers through accretion reactions makes it inadequate to compare yields of HOM dimers and HOM monomers. However, identification of HOM dimers can help us identify the exact RO_2 in the OFR and confirm the conditions of secondary OH oxidation according to the number of hydrogen atoms in the molecules.

Overall, we argue that we focused on the detailed formulae of stabilized products and confirmed the extensive existence of secondary OH oxidation through the OFR experiments. Our experimental results can be taken as reference to characterize chemical behaviors of HOMs in the atmosphere. Yields of Organonitrates and HOM dimers have been altered in our experiments, whilst their formulae clearly confirm their generation pathways and the significance of secondary OH oxidation. We acknowledge that our previous discussion on yields of HOMs in the original manuscript could be misleading, and thus we have removed those contents in the revised manuscript.

In addition, our settings are much closer to the true ambient compared to the three studies listed by Reviewer #1.

The Wang et al. (2017) study did not provide detailed concentrations of aromatic precursors and generated extremely low concentrations of OH ($(2.4 – 53) \times 10^4$ molecule cm^{-3}) by ozonolysis of tetramethylethylene in their study. Almost no HO_2 were formed in the flow tube, which made the termination of RO_2 very slow when comparing to the unimolecular reactions.

The OH concentrations in our OFR experiments, i.e., $1.09\times10^8 – 1.57\times10^9$ molecule cm^{-3}, are close to those in the Garmash et al. (2020) chamber experiments, which were in the range of $1.2\times10^7 – 4.5\times10^8$ molecule cm^{-3}. The much higher residence time in their experiments (48 min) than ours (53 s) makes the OH dose in our experiments much lower than theirs. Secondary OH reactions of stabilized first-generation products in their system is likely more favorable than ours. The Garmash et al. (2020) study did not provide a detailed estimation on concentrations of RO_2 and HO_2 in their experiments. However, according to their results, the termination products were dominated by -OOH, indicating the existence of a high HO_2 concentration. Meanwhile, the ratio between toluene-derived monomers and dimers detected by their nitrate-CIMS was 0.66, indicating a high RO_2 concentration that favors accretion reactions in their experiments. The high concentration of precursors (~ 400 ppm benzene/ ~ 25 ppm toluene/ ~ 0.4 ppm naphthalene) in their 'University of Helsinki flow reactor' also likely resulted in an extremely high RO_2 condition.

Compared to the Molteni et al. (2018) study, our experiments are generally much closer to the true ambient. Their OH concentrations in the 1,3,5-TMB oxidation experiments are around 7×10^5 molecule cm^{-3}. On the other hand, their extremely high HO_2 concentrations, i.e., 8×10^9 molecule cm^{-3}, resulted in a HO_2/OH of 20000 and led to a much earlier RO_2 termination.

All the three studies utilized oxidation products observed in the OFR or chambers as evidence to derive reaction mechanisms (Garmash et al., 2020; Wang et al., 2017; Molteni et al., 2018), though Wang et al. (2017) used extra supports from quantum chemical calculations. We believe that our results are relevant and provide further insights into the oxidation mechanisms of aromatics. On the other hand, our experiments fill in the gap of oxidation of aromatics under an intraday OH exposure.

We have revised our manuscript to include in the above argument, which reads,

2. Methods. (Line 252-295)

To validate our settings, a PAM chemistry model (PAM_chem_v8), utilized widely in previous studies, were chosen with the latest updates to calculate radical profiles in our OFR (Li et al., 2015; Cheng et al., 2021; Wang et al., 2020; Mehra et al., 2020; Lambe et al., 2015, 2018; Peng and Jimenez, 2020; Lambe et al., 2017). This model is based on a photochemical box model that includes chemistry of photolysis of oxygen, water vapor, and other trace gases by the primary wavelengths of mercury lamps, and simplified VOC and RO_2 chemistry (Table S2), but further reactions of the first-generation stabilized products and the second-generation organic radicals are not considered. The detailed reactions involved with RO_2 include:

$$RO_2 + R'O_2 \rightarrow RO + R'O + O_2 \quad (R1)$$
$$RO_2 + R'O_2 \rightarrow R=O + R'OH + O_2 \quad (R2)$$
$$RO_2 + R'O_2 \rightarrow ROH + R'=O + O_2 \quad (R3)$$
$$RO_2 + R'O_2 \rightarrow ROOR' + O_2 \quad (R4)$$
$$RO_2 + HO_2 \rightarrow ROOH + O_2 \quad (R5)$$
$$RO_2 + OH \rightarrow Products \quad (R6)$$
$$RO_2 \xrightarrow{isomerization} Products \quad (R7)$$
$$RO_2 + NO \rightarrow RO + NO_2 \quad (R8)$$
$$RO_2 + NO \rightarrow RONO_2 \quad (R9)$$
$$RO_2 \rightarrow physical\ loss \quad (R10)$$

$R1$, $R2$, and $R3$ are reactions of $RO_2 + RO_2$, forming alkoxy radicals, carbonyl termination products, and hydroxyl termination products, respectively. $R4$ is the accretion reaction, forming dimers via combination of two monomeric RO_2. $R5$ is the reaction between RO_2 and HO_2, forming hydroperoxyl radicals. $R6$ is the reaction between OH and RO_2, whose reaction products are proposed with a reference from the previous studies concluded in Table S3. $R7$ is the unimolecular reactions of RO_2 in the PAM OFR, among which the autoxidation reaction rate is the most significant. $R8$ and $R9$ are the reactions between NO and RO_2, generating alkoxy radicals and organonitrates, respectively. $R10$ is the physical loss of RO_2.

Reactions in the modified PAM_chem_v8 and their detailed kinetics are provided in Table S2. Kinetic data are obtained from the IUPAC (International Union of Pure and Applied Chemistry) dataset (https://iupac-aeris.ipsl.fr, last access: 26 October 2023) and the MCM dataset (MCM v3.3.1, https://mcm.york.ac.uk/MCM/, last access: 9 October 2023), except those that are specifically discussed in details in the supplement. Note that the total RO_2 concentration is simplified to be the sum of concentrations of BPR and $C_9H_{13}O_7$·. In this work, the autoxidation reaction and the accretion reaction of 1,3,5-TMB-derived BPR, as well as the subsequent reactions of the autoxidation product of BPR, i.e., $C_9H_{13}O_7$·, are newly implemented or modified in this model (Reaction No. 41 – 57 in Table S2). The newly implemented or modified reactions in this model are discussed in Supplementary Text S1. NO_x-related reactions are also included in the model. When we simulate experiments without NOx, these reactions do not contribute to the simulation results.

The input parameters of temperature, mean residence time, water vapor concentration, O_3 concentration, and the initial 1,3,5-TMB concentration are 25 °C, 53 s, 0.8%, 500 ppbv, and 50 ppbv, respectively, as measured directly in the experiments. The actinic flux at 254 nm, I_{254}, is constrained by comparing OH exposures by model output and OH exposures estimated by the consumption of

1,3,5-TMB as measured by a Vocus PTR. Consumption of O_3 estimated by the model agrees well with the measured results, with discrepancies being always within 10% at different OH exposures.

3. Results and discussions. (Line 297 – 363):

3.1 Validation of experimental settings

Concentration profiles of OH, RO_2, and HO_2 as a function of OH exposures in our experiments without NO_x are illustrated in Figure S1a. According to the modified PAM_chem_v8, when OH increased from 1.09×10^8 to 1.57×10^9 molecule cm^{-3}, HO_2 concentrations increased from 7.72×10^8 to 3.18×10^9 molecule cm^{-3}, whereas RO_2 concentrations increased from 4.83×10^9 to 8.48×10^9 molecule cm^{-3}. The radical concentrations in experiments with NO_x (Figure S1b) varied in a similar range, with RO_2 ranging from 3.89×10^9 to 9.34×10^9 molecule cm^{-3}, HO_2 ranging from 3.66×10^9 to 6.82×10^9 molecule cm^{-3}, and OH ranging from 4.83×10^8 to 9.05×10^8 molecule cm^{-3}, respectively. The ratios between HO_2/OH and RO_2/OH in our experiments are displayed in Figure S1c. The HO_2/OH ratio ranged between 1.9 and 7.1 in our PAM OFR experiments without NO_x, and the RO_2/OH ratio ranged between 4.9 and 47.9. In experiments with NO_x, the HO_2/OH ratio ranged between 3.7 and 17.9, whilst the RO_2/OH ratio ranged between 4.0 and 13.2. A recent comprehensive ambient campaign conducted in the wintertime central Beijing reported mean daytime peak concentrations of 8.8×10^7, 3.9×10^7, and 2.7×10^6 molecule cm^{-3} for total RO_2, HO_2, and OH, respectively (Slater et al., 2020), which corresponds to ambient RO_2/OH and HO_2/OH ratios of 32.6 and 14.4 (Figure S1c), respectively. Therefore, radical ratios in our flow tube were generally in the same order of magnitude with the ambient conditions.

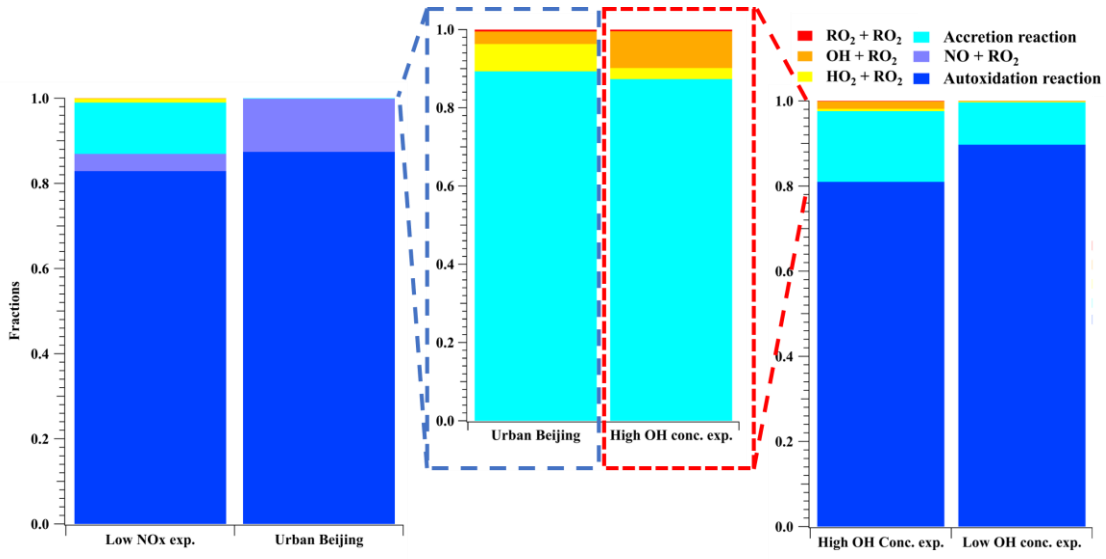

Figure 1. Fates of RO_2 generated in the low NO_x experiment (Exp. 44), urban Beijing (Slater et al., 2020), low OH and zero NO_x experiment (Exp. 19), and high OH and zero NO_x experiment (Exp. 12). Note that RO_2 fates of RO_2, OH, HO_2, and accretion channels are blown up for a better comparison for urban Beijing and the high OH and zero NO_x experiment. Reactions and kinetic rate coefficients used in the calculations are provided in Table S2.

We take Exp. 12, 19 and 44 as representative examples and compare simulation results with those from the ambient environment (Slater et al., 2020). The RO_2 lifetime in urban Beijing (Slater

et al., 2020), low NO_x experiment, low OH and zero NO_x experiment, and high OH and zero NO_x concentration experiment was 1.0, 0.7, 1.2, and 0.6 s, respectively. As shown in Figure 1, In the low NO_x experiment (Exp. 44), the fractions of RO_2 + RO_2 ($R1 - R3$), accretion reaction ($R4$), RO_2 + HO_2 ($R5$), RO_2 + OH ($R6$), autoxidation ($R7$), and RO_2 + NO ($R8 - R9$) were 0.06%, 12.1%, 0.9%, 0.07%, 82.9%, and 4.0%, respectively. Calculated based on the mean daytime peak concentrations of radicals in Beijing (Slater et al., 2020), the fractions of $R1 - R3$, $R4$, $R5$, $R6$, $R7$, and $R8 - R9$ were 0.0005%, 0.09%, 0.007%, 0.003%, 87.4%, and 12.5%, respectively. For the experiment with low OH and zero NO_x (Exp. 19), the fractions of $R1 - R3$, $R4$, $R5$, $R6$, and $R7$ were 0.05%, 10.0%, 0.15%, 0.14%, and 89.7%, respectively. For the one with high OH and zero NO_x (Exp. 12), the fractions of $R1 - R3$, $R4$, $R5$, $R6$, and $R7$ were 0.08%, 16.6%, 0.54%, 1.8%, and 81.0%, respectively. The overall lifetimes of RO_2 and the fractions of autooxidation together determine the significant and similar roles of autoxidation in both laboratory experiments and the ambient. Therefore, the autoxidation chain will run to a similar oxidation level between the laboratory and the ambient.

In experiments with NO_x (e.g., Exp. 44), though the yields of organonitrates were lower in the laboratory experiments, the formation pathways of these compounds were the same as those in the ambient. Based on the formulae of organonitrates, the detailed formulae for monomer RO_2 could be probed, which helps to investigate the existence of multi-generation OH oxidation. Alkoxy radicals generated in the NO termination channel will unlikely influence the distributions of C9 stabilized products since they tend to get decomposed in the subsequent reactions, as discussed in the Supplementary Text S1.

In experiments in absence of NO_x (e.g., Exp. 12 and 19), the proportions of $R8$ - $R9$, i.e., the NO channel in urban environment were reassigned to termination reactions of $R1$ - $R6$, i.e., RO_2 + RO_2, accretion reaction, RO_2 + HO_2, and RO_2 + OH. Comparison of relative fractions of RO_2 fates of RO_2, OH, HO_2, and accretion channels (Figure 1) shows similarities between laboratory and ambient results. By expanding proportions of these termination reactions, laboratory investigations on distributions of products can be facilitated, as the detection of certain HOM products became more precise and the mass spectra became simplified. As discussed in the "results" session, products of $R2$, $R3$, and $R5$ channels of the main BPR were not detected in our experiments due to their low oxygen contents, while secondary products between products of $R2$, $R3$, and $R5$ channels of the main BPR and OH were observed. Together with stabilized products and secondary products from $C_9H_{13}O_7$· (the peroxy radical formed from autooxidation of BPR), secondary products between products of $R2$, $R3$, and $R5$ channels of the main BPR and OH help to elucidate the first- and multi-generation reaction pathways in the 1,3,5-TMB+OH system, according to their molecular formular.

On the other hand, the much-expanded proportion of HOM dimers through accretion reactions makes it inadequate to compare yields of HOM dimers and HOM monomers. However, identification of HOM dimers can help us identify the exact RO_2 in the OFR and confirm the conditions of secondary OH oxidation according to the number of hydrogen atoms in the molecules.

Supplement:

Text S1. Introduction of the newly implemented and modified reactions in PAM model.

To better illustrate and evaluate the chemistry in the PAM OFR in our experiments, a PAM chemistry model (PAM_chem_v8), utilized widely in previous studies, is chosen with the latest updates to calculate radical profiles in our OFR (Li et al., 2015; Cheng et al., 2021; Wang et al.,

2020; Mehra et al., 2020; Lambe et al., 2015, 2018; Peng and Jimenez, 2020; Lambe et al., 2017). In this work, autoxidation and accretion of 1,3,5-TMB-derived BPR, as well as the subsequent reactions of the autoxidation product of BPR, i.e., $C_9H_{13}O_7$·, are newly implemented or modified in this model (Reaction No. 42 – 58 in Table S2). The pathways of the peroxy radicals and their kinetics are discussed below. NO_x-related reactions are also included in the model. When we simulate experiments without NO_x, these reactions do not contribute to the simulation results.

RO_2 can react with a number of radicals, generating termination products or other radicals.

$$RO_2 + R'O_2 \rightarrow RO + R'O + O_2 \quad (R1)$$

$$RO_2 + R'O_2 \rightarrow R=O + R'OH + O_2 \quad (R2)$$

$$RO_2 + R'O_2 \rightarrow ROH + R'=O + O_2 \quad (R3)$$

$$RO_2 + R'O_2 \rightarrow ROOR' + O_2 \quad (R4)$$

$$RO_2 + HO_2 \rightarrow ROOH + O_2 \quad (R5)$$

$R1$, $R2$, and $R3$ are reactions of RO_2 + RO_2, forming alkoxy radicals, carbonyl termination products, and hydroxyl termination products, respectively. $R4$ is an accretion reaction, forming dimers via combination of two monomeric RO_2. $R5$ is the reaction between RO_2 and HO_2, forming hydroperoxyl radicals. The reaction rate constants for RO_2 in $R1$ – $R5$ were obtained by MCM or previous investigations (e.g., Jenkin et al., 2003; Berndt et al., 2018; Peng and Jimenez, 2020). We treat $R1$ – $R3$ as a total reaction with a reaction rate constant of 8.8×10^{-13} molecule^{-1} cm^3 s^{-1}, and branching ratios of $R1 - R3$ of 0.6, 0.2, and 0.2, respectively, as suggested by MCM (Jenkin et al., 2003). The reaction rate constants of BPR and $C_9H_{13}O_7$· for $R4$ are 1.7×10^{-10} and 2.6×10^{-10} molecule^{-1} cm^3 s^{-1}, respectively (Berndt et al., 2018). The reaction rate constants for $R5$ is 1.5×10^{-11} molecule^{-1} cm^3 s^{-1} (Jenkin et al., 2003).

$$RO_2 + OH \rightarrow Products \quad (R6)$$

$R6$ is the reaction between OH and RO_2. The reaction rate constant for $R6$ is 1×10^{-10} molecule^{-1} cm^3 s^{-1} according to previous studies (Bossolasco et al., 2014; Yan et al., 2016; Assaf et al., 2016, 2017; Peng and Jimenez, 2020). Current knowledge on the reaction products for the reaction of CH_3O_2· + OH, the most studied RO_2 + OH reaction, is summarized in Table S3. The products of this reaction are suggested to include a Criegee intermediate (CH_2O_2·), a stabilized methylhydrotrioxide (CH_3OOOH), an alkoxy radical (CH_3O·), and methanol (CH_3OH) (Yan et al., 2016; Fittschen, 2019; Caravan et al., 2018; Müller et al., 2016). Müller et al. (2016) and Caravan et al. (2018) suggest that the formation of CH_2O_2· is actually infeasible, and Yan et al. (2016) estimated an upper limit branching ratio of 5% for this pathway. The branching ratios of stabilized products CH_3OH and CH_3OOOH are 6 - 7% (Caravan et al., 2018; Müller et al., 2016) and 7% (Müller et al., 2016), respectively. The most significant product of this reaction is the alkoxy radical (CH_3O·), with a branching ratio of more than 86% (Müller et al., 2016). In the absence of NO_x, CH_3OH and CH_3O· can also be formed via the traditional unimolecular reaction between CH_3O_2· and RO_2, i.e., $R1$ and $R3$. The possible role of this reaction of large RO_2, i.e., BPR and other C9-RO_2, with OH has not yet been investigated. However, according to the branching ratios for the reaction of CH_3O_2· + OH, this reaction is likely to form RO instead of stabilized C9 products. Hence, we assume that the branching ratios of hydrotrioxide (ROOOH), RO, and ROH are 0.07, 0.86, and 0.07, respectively, for BPR + OH and C9-RO_2 + OH.

$$RO_2 \xrightarrow{isomerization} Products \quad (R7)$$

Unimolecular reactions can also contribute to consumption of RO_2 in the PAM OFR. RO_2

isomerization rate coefficients are highly dependent on their structures, spanning from 10^{-3} - 10^{6} s^{-1} (Bianchi et al., 2019; Crounse et al., 2013; Knap and Jørgensen, 2017; Praske et al., 2018). However, only some substituted acyl RO_2 can undergo rapid isomerization at a reaction rate of 10^{6} s^{-1} (Knap and Jørgensen, 2017). 1,3,5-TMB-derived BPR and its autoxidation product, $C_9H_{13}O_7\cdot$, do not belong to the group of substituted acyl RO_2 (Molteni et al., 2018; Tsiligiannis et al., 2019). The most important unimolecular reactions for 1,3,5-TMB-derived BPR is likely autoxidation while the precise autoxidation reaction rates of 1,3,5-TMB-derived BPR and other RO_2 in this system are currently unclear (Bianchi et al., 2019; Molteni et al., 2018). Previous theoretical investigations suggest that more than 90% BPR generated by the oxidation of 1,3,5-TMB possess a structure favoring autoxidation and thus their overall autoxidation reaction rate is relatively fast (Wang et al., 2017). Laboratory experiments also indicate a higher HOM molar yield for 1,3,5-TMB than ethylbenzene and xylenes (Molteni et al., 2018). We arbitrarily set the autoxidation reaction rate of 1,3,5-TMB-derived BPR the same as that of ethylbenzene-derived BPR, i.e., 7.0 s^{-1}, as a lower limit to estimate the fate of 1,3,5-TMB-derived RO_2 (Wang et al., 2017). Indeed, this value is not necessarily appropriate for all the RO_2 in this system and this estimation is a simplified result mainly based on the most important RO_2 in the oxidation of 1,3,5-TMB, i.e., BPR. Meanwhile, this value will not influence the total concentration of RO_2 but the concentration of BPR, as the total RO_2 concentration is simplified to be the sum of concentrations of BPR and $C_9H_{13}O_7\cdot$.

Especially, because RO_2 in our experiments mainly consists of RO_2 with multiple oxygenated functionalities and high carbon contents, i.e., BPR and its isomerization products, which can undergo accretion reactions rapidly as fast as 10^{-10} $molecule^{-1}$ cm^3 s^{-1}. However, only around 50% RO_2 in the atmosphere are typically derived from aromatics and long-chain-alkanes containing carbon atoms larger than 4 that can undertake accretion reactions at a considerable reaction rate coefficient (Berndt et al., 2018; Bianchi et al., 2019), as observed in Beijing (Slater et al., 2020; Tan et al., 2018). Therefore, the proportion of accretion reaction in the ambient was calculated with half of the reaction rate coefficient, i.e., 8.5×10^{-11} $molecule^{-1}$ cm^3 s^{-1}. The reactions between NO and RO_2 can generate alkoxy radicals similar to $R1$ and organonitrates, which are regarded as $R9$ and $R10$.

$$RO_2 + NO \rightarrow RO + NO_2 \qquad (R8)$$

$$RO_2 + NO \rightarrow RONO_2 \qquad (R9)$$

The reaction rate for the sum of these two reactions is 8.5×10^{-12} $molecule^{-1}$ cm^3 s^{-1}. The branching ratios of these two reactions are 0.843 and 0.157, respectively, according to MCM (Jenkin et al., 2003).

Alkoxy radicals, RO, will be generated in $R1$, $R6$, and $R8$. The widely used near-explicit mechanism, MCM, assumes that RO formed via the alkoxy channel of BPR ($R1$) will decompose into small molecules. Recently, Xu et al. (2020) probed the chemical fates of BPR-derived RO, hereafter referred to as bicyclic alkoxy radical (BCP-oxy), in the oxidation of benzene by laboratory experiments and model calculations, which can be taken as a reference to induce the mechanism of 135-TMB-derived BCP-oxy. BCP-oxy can undergo two reactions, i.e., ring-breakage and ring-closure, and a new calculation result suggests that the branching ratio of ring-breakage reaction is larger than 98% (Wang et al., 2013). 56% of ring-breakage reactions will break benzene-derived BCP-oxy into butenedial and glyoxal, and the rest 44% will generate a C6 alkyl radical by the 1,5-aldehydic H-shift. The latter C6 alkyl radical will further undergo other reactions, including a 93% branching ratio for decomposition reactions that results in a reduction of carbon atom number (Xu

et al., 2020). Therefore, most of benzene-derived BCP-oxy will likely decompose into compounds with fewer carbon atoms. We assume that 1,3,5-TMB-derived BCP-oxy will undertake these decomposition reactions with a similar branching ratio, which means that these radicals cannot form a large number of stabilized products that can influence the distributions of stabilized C9 products in nitrate CIMS.

The physical loss of RO_2 in the PAM OFR consists of the condensation loss to the aerosol particles and the diffusion loss to the OFR walls, which can be regarded as $R10$.

$$RO_2 \rightarrow physical\ loss \qquad (R10)$$

In our experiments, measurement results by a long-SMPS show that the aerosol particles presented in the PAM OFR were few and thus the condensation loss of HOMs to the aerosol particles was minor and not further considered. The first-order loss rate of HOMs to the OFR walls, k_{wall}, is limited by eddy diffusion and can be calculated with the following function (Cheng et al., 2021; Palm et al., 2016; McMurry and Grosjean, 1985):

$$k_{wall} = \frac{A}{V} \cdot \frac{2}{\pi} \cdot \sqrt{k_e D_g} \qquad (Eq1)$$

where the OFR surface-area-volume ratio (A/V) is 25 m^{-1} and the coefficient of eddy diffusion (k_e) is 0.0042 s^{-1}, as estimated by the method utilized in a previous study (Brune, 2019) and given in $Eq2$.

$$k_e = 0.004 + 10^{-2.25} V^{0.74} \qquad (Eq2)$$

V is the enclosure volume (m^3). The molecular diffusion coefficient, D_g, is estimated with the method as described by Fuller et al. (1966) and is around 5×10^{-6} m^2 s^{-1} with 1,3,5-TMB derived BPR as an example. Hence, k_{wall} is around 0.0023 s^{-1} in the PAM OFR.

(a)

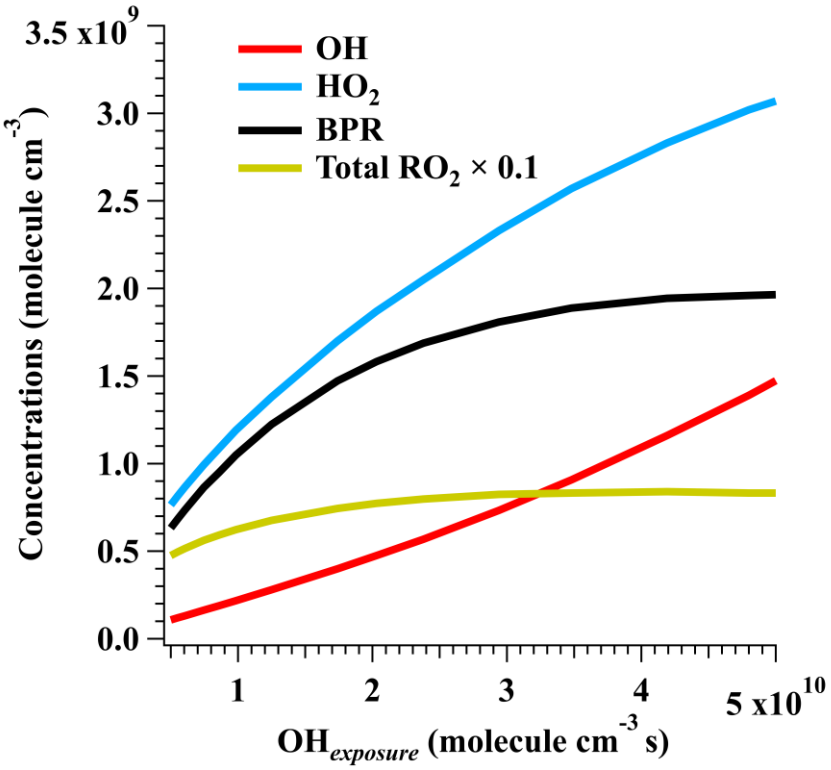

(b)

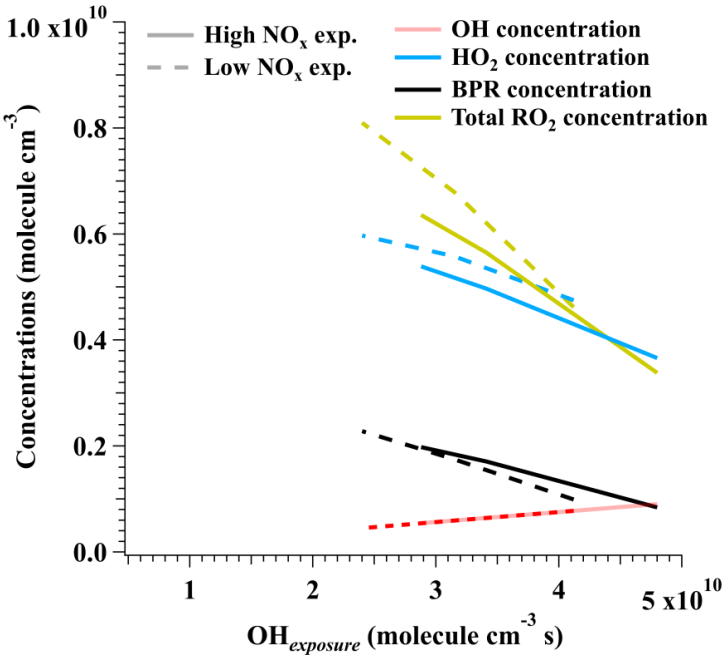

(c)

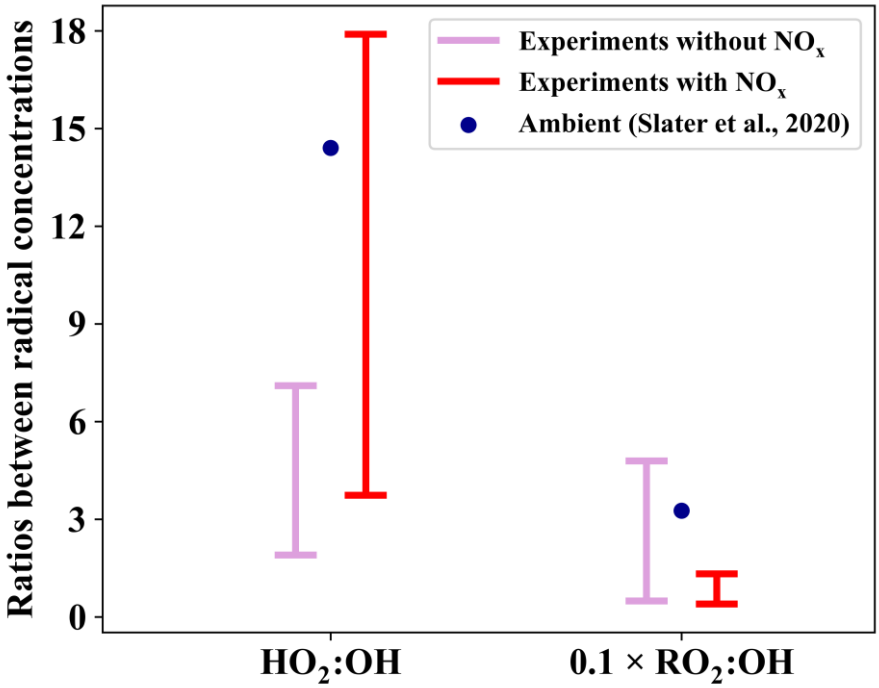

Figure S1. (a) Concentration profiles of OH, HO_2, BPR, and total RO_2 in the PAM OFR as a function of OH exposures. The average total concentrations of RO_2 were scaled with a factor of 0.1 for a better visualization. (b) HO_2/OH, RO_2×0.1/OH, and their ambient values. The ambient values were calculated according to Slater et al. (2020).

Table S2. Reactions included in the modified PAM_chem_v8 under the settings with only 254 nm UV lights on. For experiments in the absence of NO_x, the input value of N_2O is 0 and all the NO_x-related reactions actually proceed with a zero rate. RO_2 is the sum of BPR and $C_9H_{13}O_7$· for simplification.

No	Reactions	Reaction rate constants/photolysis rate (molecule^{-1} cm^3 s^{-1}/ s^{-1})
1	$HO_2 + h\nu$ (λ = 254 nm) = OH + O(^{1}D)	$2.63\times10^{-19}\times flux_{254}$
2	$O_3 + O(^1D) = 2O_2$	1.20×10^{-10}
3	$O_3 + O(^1D) = O + O + O_2$	1.20×10^{-10}
4	$O + OH = H + O_2$	$2.20\times10^{-11}\times e^{120/T}$
5	$O(^1D) + H_2 = OH + H$	1.20×10^{-10}
6	$HO_2 + H = 2OH$	7.20×10^{-11}
7	$HO_2 + H = O + H_2O$	1.60×10^{-12}
8	$HO_2 + H = H_2 + O_2$	6.90×10^{-12}
9	$O_3 + H = OH + O_2$	$1.40\times10^{-11}\times e^{-470/T}$
10	$N_2O + O(^1D) = 2NO$	$6.70\times10^{-11}\times e^{20/T}$
11	$N_2O + O(^1D) = N_2 + O_2$	$4.70\times10^{-11}\times e^{20/T}$
12	$O + HO_2 = OH + O_2$	$3.02\times10^{-11}\times e^{200/T}$
13	$O + H_2O_2 = OH + HO_2$	$1.40\times10^{-12}\times e^{-2000/T}$
14	$O + O_3 = 2O_2$	$8.00\times10^{-12}\times e^{-2060/T}$
15	$O + NO_3 = NO_2 + O_2$	1.00×10^{-11}
16	$O + NO_2 = NO + O_2$	$5.12\times10^{-12}\times e^{210/T}$
17	$OH + O_3 = HO_2 + O_2$	$1.70\times10^{-12}\times e^{-940/T}$
18	$OH + HO_2 = H_2O + O_2$	$4.80\times10^{-11}\times e^{250/T}$
19	$OH + HONO = H_2O + NO_2$	$1.80\times10^{-11}\times e^{-390/T}$
20	$OH + H_2O_2 = H_2O + HO_2$	$2.90\times10^{-12}\times e^{-160/T}$
21	$OH + H_2 = H_2O + H$	$2.80\times10^{-12}\times e^{-1800/T}$
22	$OH + OH = H_2O + O$	1.80×10^{-12}
23	$HO_2 + O_3 = OH + O_2$	$1.00\times10^{-14}\times e^{-490/T}$
24	$HO_2 + NO = OH + NO_2$	$3.50\times10^{-12}\times e^{270/T}$
25	$NO + O_3 = NO_2 + O_2$	$2.00\times10^{-12}\times e^{-1400/T}$
26	$NO_2 + O_3 = NO_3 + O_2$	$1.20\times10^{-13}\times e^{-2450/T}$
27	$NO + NO_3 = 2NO + O_2$	$1.50\times10^{-11}\times e^{170/T}$
28	$NO_3 + NO_3 = 2NO_2 + O_2$	$8.50\times10^{-13}\times e^{-2450/T}$
29	$N_2O_5 + H_2O = 2HNO_3$	2.00×10^{-21}
30	$O + O_2 + M = O_3 + M$	$6.00\times10^{-34}\times M\times(300/T)^{2.4}$
31	$H + O_2 + M = HO_2 + M$	$k_o = 4.40\times10^{-32}\times M\times(300/T)^{1.3}$ $k_h = 7.50\times10^{-11}\times(300/T)^{0.2}$ $k = k_o/(1+(k_o/k_h))\times0.6^{(1+(\log10(k_o/k_h))^{-2}}$
32	$OH + OH + M = H_2O_2 + M$	$k_o = 6.90\times10^{-31}\times M\times(300/T)$ $k_h = 2.60\times10^{-11}$ $k = k_o/(1+(k_o/k_h))\times0.6^{(1+(\log10(k_o/k_h))^{-2}}$
33	$OH + NO + M = HONO + M$	$k_o = 7.00\times10^{-31}\times M\times(300/T)^{2.6}$ $k_h = 3.60\times10^{-11}\times(300/T)^{0.1}$ $k = k_o/(1+(k_o/k_h))\times0.6^{(1+(\log10(k_o/k_h))^{-2}}$
34	$OH + NO_2 + M = HNO_3 + M$	$k_o = 1.80\times10^{-30}\times M\times(300/T)^{2.6}$ $k_h = 2.80\times10^{-11}$ $k = k_o/(1+(k_o/k_h))\times0.6^{(1+(\log10(k_o/k_h))^{-2}}$
35	$OH + HNO_3 = H_2O + NO_3$	$k_{00} = 2.40\times10^{-14}\times e^{460/T}$ $k_{01} = 6.50\times10^{-34}\times e^{2199/T}$ $k_{02} = 2.80\times10^{-11}\times e^{-2450/T}$ $k = k_{00} + (k_{01}\times M)/(1+(k_{01}\times M)/k_{02})$
36	$HO_2 + NO_2 + M = HO_2NO_2 + M$	$k_o = 1.80\times10^{-31}\times M\times(300/T)^{3.2}$ $k_h = 4.70\times10^{-12}\times(300/T)^{1.4}$ $k = k_o/(1+(k_o/k_h))\times0.6^{(1+(\log10(k_o/k_h))^{-2}}$ $k_{reverse} = k/(2.10\times10^{-27}\times e^{10900/T})$
37	$NO_2 + NO_3 + M = N_2O_5 + M$	$k_o = 2.00\times10^{-30}\times M\times(300/T)^{4.4}$ $k_h = 1.40\times10^{-12}\times(300/T)^{0.7}$ $k = k_o/(1+(k_o/k_h))\times0.6^{(1+(\log10(k_o/k_h))^{-2}}$

		$k_{reverse} = k /(2.70\times10^{-27}\times e^{11000/T})$
38	OH + HNO_4 = products	$1.30\times10^{-12}\times e^{250/T}$
39	Sci + H_2O = products	4.00×10^{-15}
40	1,3,5-TMB + OH = BPR	$0.8\times5.67\times10^{-11}$
41	1,3,5-TMB + OH = Products	$0.2\times5.67\times10^{-11}$
42	BPR = C9H13O7	7
43	BPR + RO_2 = ROOR'	1.70×10^{-10}
44	BPR + RO_2 = R=O/ROH + O_2	$0.4\times8.8\times10^{-13}$
45	BPR + RO_2 = 2RO + O_2	$0.6\times8.8\times10^{-13}$
46	BPR + OH = RPO_2 + H_2O	1.00×10^{-10}
47	BPR + HO_2 = ROOH + O_2	1.20×10^{-11}
48	BPR = wall loss	0.0023
49	BPR + NO = RO + NO_2	$0.843\times8.50\times10^{-12}$
50	BPR + NO + M = $RONO_2$+ M	$0.157\times8.50\times10^{-12}$
51	C9H13O7 + RO_2 = ROOR'	2.60×10^{-10}
52	C9H13O7 + RO_2 = R=O/ROH + O_2	$0.4\times8.8\times10^{-13}$
53	C9H13O7 + RO_2 = 2RO + O_2	$0.6\times8.8\times10^{-13}$
54	C9H13O7 + OH = RPO_2 + H_2O	1.00×10^{-10}
55	C9H13O7 + HO_2 = ROOH + O_2	1.20×10^{-11}
56	C9H13O7 = wall loss	0.0023
57	C9H13O7+ NO = RO + NO_2	$0.843\times8.50\times10^{-12}$
58	C9H13O7 + NO + M = $RONO_2$+ M	$0.157\times8.50\times10^{-12}$
59	ROOH + OH = RO_2 + H_2O	$5.30\times10^{-12}\times e^{190/T}\times0.6$
60	ROOH + OH = RPHO + OH + H_2O	$5.30\times10^{-12}\times e^{190/T}\times0.4$
61	RO + O_2 = RPO + HO_2	6.00×10^{-15}
62	H_2O_2 + *hv* (λ = 254 nm) = 2OH	$6.70\times10^{-20}\times flux_{254}$
63	NO_2 + *hv* (λ = 254 nm) = O + NO	$1.00\times10^{-20}\times flux_{254}$
64	HONO + *hv* (λ = 254 nm) = OH + NO	$1.40\times10^{-19}\times flux_{254}$
65	HNO_3 + *hv* (λ = 254 nm) = OH + NO_2	$1.95\times10^{-20}\times flux_{254}$
66	HNO_4 + *hv* (λ = 254 nm) = HO_2 + NO_2	$3.60\times10^{-19}\times flux_{254}$
67	N_2O_5 + *hv* (λ = 254 nm) = NO_2 + NO_3	$3.20\times10^{-19}\times flux_{254}$

Table S3. The branching ratios of different pathways for $CH_3O_2\cdot$ + OH.

Reactions	Branching ratio	References
$CH_3O_2\cdot$ + OH → $CH_2O_2\cdot$ + H_2O	< 5%	(Yan et al., 2016)
	0	(Caravan et al., 2018; Müller et al., 2016)
$CH_3O_2\cdot$ + OH → $CH_3O\cdot$ + HO_2	86%	(Müller et al., 2016)
$CH_3O_2\cdot$ + OH → CH_3OH + HO_2	6 ± 2%	(Caravan et al., 2018)
	7%	(Müller et al., 2016)
$CH_3O_2\cdot$ + OH → CH_3OOOH	7%	(Müller et al., 2016)

Q 1.2 What is the influence of aromatic photochemistry in your PAM setup? Aromatics are known to strongly absorb light at relatively long wavelengths, and the oxygenated aromatics even more (see e.g., https://www.uv-vis-spectral-atlas-mainz.org/uvvis/), so I'm wondering how was the relevance of the used light sources tested in this work? This is not irrelevant for aromatic oxidation.

Response 1.2:

Peng et al. (2016) evaluated the relative significance of photolysis of 1,3,5-TMB in the OFR.

The absorption cross-sections of 1,3,5-TMB at 254 nm is 3.68×10^{-19} cm^2 (Keller-Rudek et al., 2013). For our experiments in the absence of NO_x, UV photon fluxes at 254 nm are estimated to range from 5.6×10^{14} to 2.5×10^{15} photons cm^{-2} s^{-1} based on the modified PAM_chem_v8. The photolysis rate of 1,3,5-TMB is estimated to range between 2.1×10^{-4} and 9.2×10^{-4} s^{-1}. Since the OH reaction rate constant of 1,3,5-TMB is 5.67×10^{-11} $molecule^{-1}$ cm^3 s^{-1} (Jenkin et al., 2003) and the OH concentration in the OFR was in the range of 1.09×10^8 – 1.57×10^9 molecule cm^{-3}, the OH reaction rate for 1,3,5-TMB is estimated to be 6.2×10^{-3} – 8.9×10^{-2} s^{-1}. Therefore, the ratio of photolysis-to-OH reaction was merely 0.010 – 0.033. Hence, photolysis of 1,3,5-TMB was insignificant in the OFR.

For stabilized products such as HOMs, the relative significance of photolysis can be estimated based on their photolysis rates. The cross sections of organic molecules are usually ~ 3.9×10^{-18} - 3.9×10^{-17} cm^2 (Peng et al., 2016). The photolysis quantum yields of multifunctional species are unlikely to be larger than those of species with only one carbonyl and one hydroxyl, as discussed in previous studies (Peng et al., 2016; Peng and Jimenez, 2020), which are around 0.1. The UV photon fluxes at 254 nm were in the range of 5.6×10^{14} – 2.5×10^{15} photons cm^{-2} s^{-1} as stated in the above. Therefore, the photolysis rates of HOMs are estimated to range between 2.18×10^{-4} and 9.75×10^{-3} s^{-1}. The reaction rate between OH and the stabilized first-generation products are estimated to be around 1.28×10^{-10} $molecule^{-1}$ cm^3 s^{-1}, as suggested by MCM. Hence, the ratio of photolysis rates of HOMs to their secondary OH oxidation rates is estimated to be around 0.020 – 0.056. Meanwhile, photolysis of HOMs can lead to decomposition, decreasing detected signals of HOMs, but unlikely to generate new HOMs.

We have revised our manuscript (Line 177 – 189), which reads:

"Non-tropospheric VOC photolysis is a typical issue that should be taken into account when evaluating the settings of OFR laboratory experiments. Photolysis of the precursor and HOMs were evaluated, showing that photolysis was not a contributor to our observation. The photolysis rate of 1,3,5-TMB can be estimated based on the absorption cross-sections of 1,3,5-TMB at 254 nm (Keller-Rudek et al., 2013) and UV photon fluxes estimated by a chemistry model discussed in the following sections. The ratio of photolysis-to-OH reaction in our experiments was merely 0.010 – 0.033. Hence, photolysis of 1,3,5-TMB was insignificant in the OFR.

For stabilized products such as HOMs, the cross sections of organic molecules are usually ~ 3.9×10^{-18} - 3.9×10^{-17} cm^2 (Peng et al., 2016), while the reaction rate between OH and the stabilized first-generation products are estimated to be around 1.28×10^{-10} $molecule^{-1}$ cm^3 s^{-1}, as suggested by MCM (Jenkin et al., 2003). Hence, the ratio of photolysis rates of HOMs to their secondary OH oxidation rates is estimated to be merely around 0.020 – 0.056."

Q 1.3. *You used a relatively long ¼ inch Teflon sampling tube for the CIMS. This is the smallest tube diameter I've ever come across with nitrate CIMS sampling. One would expect the HOM losses, especially the most oxygenated ones, to be very significant in this tube. Nevertheless, HOM with high O-content seems to be detected with this setup too!*

Response 1.3:

In our experiments, the sample flow is sampled from the center of the reactor. This PAM design

is identical to those utilized in the Jimenez group and other groups (Li et al., 2015; Lambe et al., 2017, 2015), including the position and type of lamps, volume, and the sampling method. Transmission efficiencies for typical gases, bis(2-ethylhexyl)sebacate particles, and H_2SO_4 particles in the PAM OFR, and sampling efficiencies into sampling tubes have been well characterized in a previous study, which shows a better transmission efficiency compared to other types of flow tubes (Lambe et al., 2011). This setting also validates usage of the PAM_chem_v8 model to estimate concentrations of radicals in the OFR. We acknowledge that this is not a perfect sampling setting for nitrate CIMS. However, the reduction in the sampling efficiencies of various HOMs is like to be close, if not identical, which keeps the distribution of HOMs.

We've revised our manuscript (Line 212 - 217), which reads:

"We followed the same sampling method of PAM OFR as those in previous studies, in order to obtain a similar flow tube residence time distributions (RTDs) and thus validate usage of the modified PAM_chem_v8 model to estimate concentrations of radicals in the OFR. We acknowledge that this is not a perfect sampling setting for nitrate CIMS. However, the reduction in the sampling efficiencies of various HOMs is likely to be close, if not identical, which keeps the distributions of HOMs."

Q 1.4. *Jenkin 2003 reference does not have autoxidation.*

Response 1.4:

We use this reference to show that BPR is the main product of OH-initiated oxidation of aromatics. To avoid misunderstanding, we move this reference to a position closer to the BPR statement and add a new citation on autoxidation.

We have revised the manuscript (Line 70 - 74), which reads,

"Take alkylbenzenes as an example, previous studies suggest that the main products of OH-initiated oxidation of alkylbenzenes (C_xH_{2x-6}, x=7, 8, or 9), i.e., bicyclic peroxy radicals (BPR, $C_xH_{2x-6}O_5\cdot$, x=7, 8, or 9) (Jenkin et al., 2003), can undergo an autoxidation reaction and form a new peroxy radical, $C_xH_{2x-6}O_7\cdot$ (x=7, 8, or 9) (Wang et al., 2017)."

Q 1.5. *The autoxidation reaction of BPR by H-abstraction has been found relatively slow by Wang et al 2017, not rapid.*

Response 1.5:

We assume that Reviewer #1 was referring to the following sentence, "The autoxidation reaction of BPR could be very fast because an allylic radical will be formed after the hydrogen shift (Wang et al., 2017)." Here, We intend to discuss the intramolecular H-shift or so-called H-migration (Bianchi et al., 2019) instead of the H-abstraction by the OH.

As stated in the Wang et al. (2017) study, "The routes via R4-BPRs are particularly important because of the relatively fast H-migration". Therefore, the exact autoxidation reaction rate should depend on the detailed structures of RO_2, some of which can be fast if their structures favor autoxidation.

We have revised our manuscript (Line 78 - 79), which reads, "The autoxidation of BPR could be fast if it has a favorable structure, as found in a previous study (Wang et al., 2017)."

Q 1.6. *Several of the products detected seem to have worryingly many H-atoms in the structures. Especially the $C_9H_{17}O_m$ radicals.*

Response 1.6:

We are very sorry that we do not identify the exact molecule the referee is referring to.

In our experiments, HOM monomers typically contained 12 – 16 hydrogen atoms and HOM dimers typically contained 26 – 30 hydrogen atoms. The hydrogen atom numbers were the same as those reported in previous 1,3,5-TMB oxidation experiments (Molteni et al., 2018; Tsiligiannis et al., 2019).

As for $C_9H_{17}O_m$, we have not observed any compounds that support the existence of $C_9H_{17}O_m$ radicals (Line 296 – 304 in the original manuscript). we suggest that all the detected monomers did not possess hydrogen atoms more than 16.

Q 1.7. *How well does the relatively low NO with the high RO_2 simulate atmospheric NO_x chemistry?*

Response 1.7:

Please refer to our response 1.1

We acknowledge that the NO:RO_2 ratio in the PAM OFR is lower than typical values in the ambient atmosphere. There were two NO_x settings in our experiments, which used 1.8 ppbv NO + 70 ppbv NO_2 and 4.8 ppbv NO + 120 ppbv NO_2, respectively. Because of the existence of O_3 that was utilized to generate $O(^1D)$ in the OFR and its rapid reaction rate with NO, the NO concentration in our system was unlikely to be increased by a large content. These two sets of NO_x experiments are meant to validate the existence of multigeneration OH oxidation in the system, as proved by the existence of compounds with multiple nitrogen atoms in such a low NO:RO_2 ratio condition.

We have revised our manuscript (Line 551 - 556), which reads,

"The NO:RO_2 ratio in the PAM OFR is lower than typical values in the ambient atmosphere, which is due to the existence of O_3 that was utilized to generate $O(^1D)$ in the OFR and its rapid reaction rate with NO. However, due to rapid reaction rate constants between NO and RO_2, i.e., around 8.5×10^{-12} molecule^{-1} cm^3 s^{-1}, the reaction rate for the NO termination channel of RO_2 was as fast as around 0.3 – 1.0 s^{-1}. Large amounts of organonitrates would still be formed. Our conclusion is also valid because of detection of compounds with multiple nitrogen atoms."

Q 1.8. *"Such a slow autoxidation reaction rate cannot explain the extensive existence of HOM monomers with more than 7 oxygen atoms and HOM dimers with more than 10 oxygen atoms, which are the maximum numbers of oxygen atoms in stabilized monomer and dimer products, respectively, formed from $C_xH_{2x-6}O_7$·(Mentel et al., 2015; Molteni et al., 2018; Wang et al., 2020)." → There's a recent paper from my group that could provide an explanation what is observed here: https://www.nature.com/articles/s41467-023-40675-2*

Response 1.8:

Thanks for pointing out the latest reference.

We have revised our manuscript (Line 90 – 95), which reads,

"A very recent investigation offers new insights into the formation mechanism of these products, indicating the molecular rearrangement of BPR can initiate a series of autoxidation (Iyer

et al., 2023). However, the formation mechanism of HOMs with a large hydrogen atom number is still vague, e.g., monomer products with 16 hydrogen atoms in the OH-initiated oxidation of TMB and with 14 hydrogen atoms in the OH-initiated oxidation of xylene."

Q 1.9. *I find it confusing to draw the "double-peroxide-ring" pathways in Schemes 1 and 2, if you even explicitly mention that they are unlikely. I advise to remove them, and the text " Another possibility is the formation of a second oxygen bridge after the hydrogen shift of BPR (Molteni et al., 2018)," altogether.*

Response 1.9:

Thanks for the suggestion.

We have revised our manuscript (Line 420 - 427), which reads,

"… has two isomers. A second-step of endo-cyclization is required in the formation of one of the isomer, which is extremely slow and not competitive as shown in several previous studies using both experimental and theoretical approaches (Wang et al., 2017; Xu et al., 2020). Even if such a second O_2 bridging to a double bond is assumed to be possible, the abundance of this isomer should be significantly smaller than the other one, because of the much faster reaction rate of H-shift reaction. Therefore, we do not take the $C_9H_{13}O_7$· isomer containing a double endo-cyclization into consideration in this work. The majority of HOM monomers is generated from subsequent reactions of $C_9H_{13}O_5$· and newly formed $C_9H_{13}O_7$·, both of which contain one C=C bond in the carbon backbone and thus have a feasible site for OH addition. Meanwhile, the autoxidation reaction rate for newly formed $C_9H_{13}O_7$· should be …".

We have revised Scheme 1 as below:

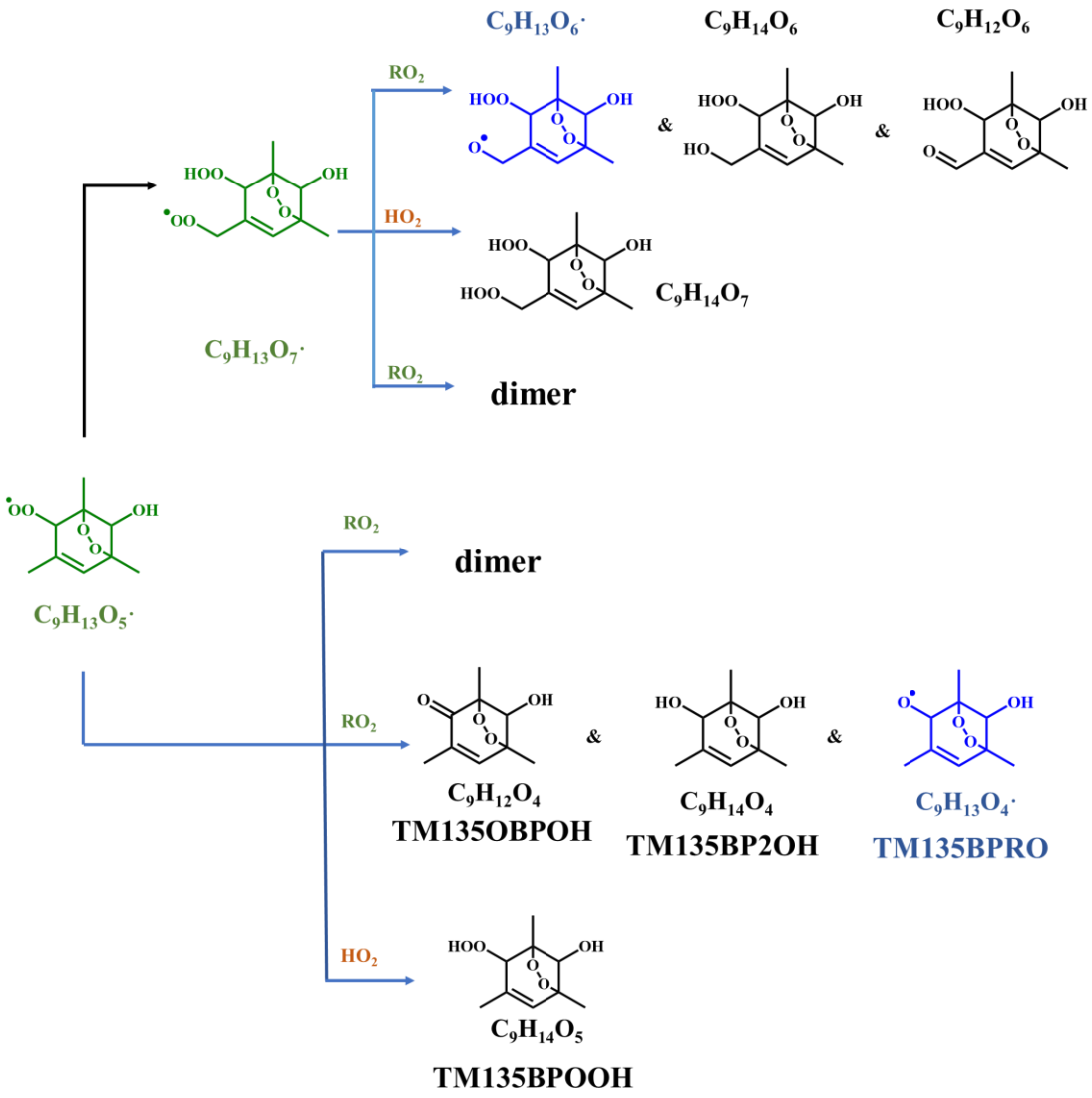

Scheme 1. Oxidation pathways of the bicyclic peroxy radical $C_9H_{13}O_5$· (MCM name: TM135BPRO2) in the OH-initiated oxidation of 1,3,5-TMB. Green, blue, and black formulae denote alkyl peroxy radicals, alkoxy radicals and stabilized products, respectively. Black arrows denote the autoxidation pathway. MCM names for HO_2- and RO_2-termination products of TM135BPRO2 are present.

We have also revised Scheme 2 (Scheme 4 in the revised manuscript) as below:

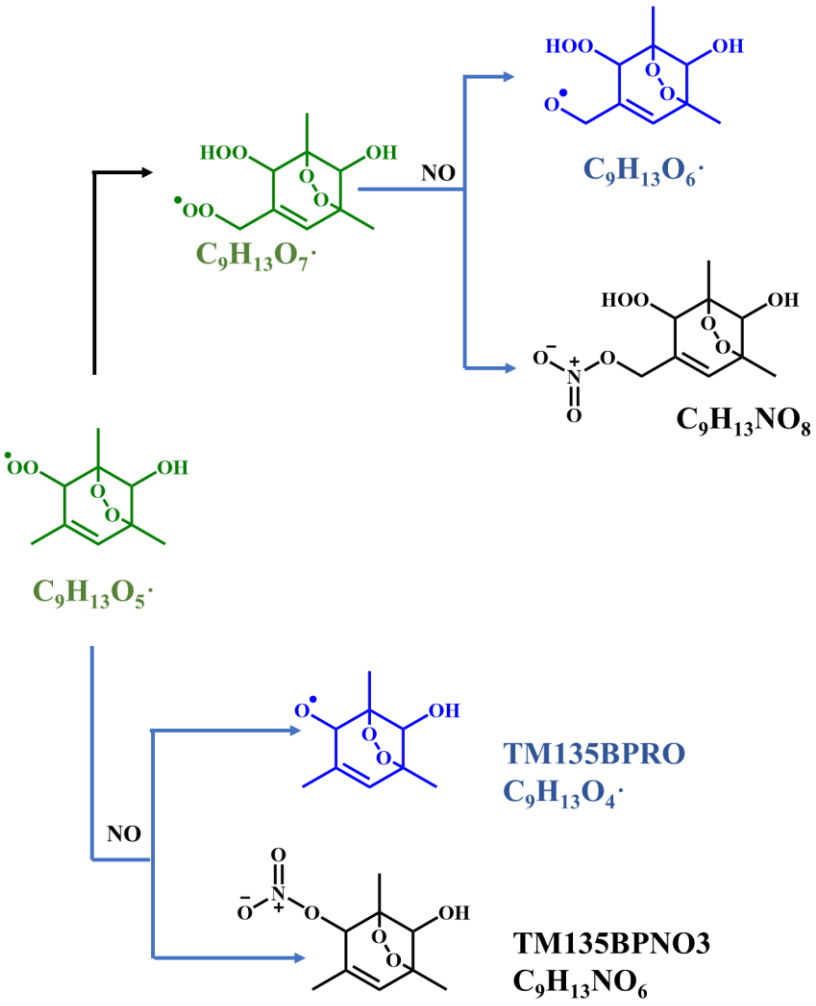

Scheme 4. NO termination reactions of the bicyclic peroxy radical $C_9H_{13}O_5·$ (MCM name: TM135BPRO2) and its autoxidation reaction products. Green, blue, and black formulae denote alkyl peroxy radicals, alkoxy radicals and stabilized products, respectively. Black arrows denote the autoxidation pathway. MCM names of NO-termination products of TM135BPRO2 are present.

Q 1.10. *"with an OH exposure equivalent to 2.4 – 19.4 days of atmospheric photochemical ageing. Certainly, such extremely high OH exposures favor secondary OH chemistry and help to facilitate our understanding on product distributions"*
→ I would argue it doesn't, except for PAM conditions. As explained above, it does matter at what order and rate different oxidation steps happen in the atmosphere, and using such a high OH doses seem to necessarily skew up the chemistry. Figure 1 seems to be a good indication of this, as the "dimers" are generated faster than the monomers, and at the higher OH dose even the sum of "dimers" decrease.

Response 1.10:

Validation of our experiments has been discussed in our Response 1.1.

The accretion reaction rate constant of 1,3,5-TMB-derived BPR has been well measured by

Berndt et al. (2018), which is around 1.7×10^{-10} molecule^{-1} cm^3 s^{-1}. They also calculated the reaction rates between RO_2 and RO_2, as well as between HO_2 and RO_2 under NO < 40 pptv, which shows that accretion reactions of BPR dominate if total concentrations of aromatics are within the range 4 – 40 ppbv. This estimation on the fates of RO_2 is similar to our experiments in the absence of NO_x. Hence, the faster formation of HOM dimers than monomers is expected, which made the maximum concentrations of HOM dimers appear earlier than HOM monomers. However, this study is not meant to compare HOM monomer and HOM dimer signals crossly here, but to pay attention to their formulae.

In order to avoid misunderstanding, we have revised our manuscript (Line 370 - 373), which reads,

"… The most abundant HOM products are also shown in stack in Figure 2, whose relationships with OH exposures are superimposed by …"

(Line 384 - 389), which reads,

"Because of the inherent disadvantage of laboratory experiments, RO_2 concentrations are always too high in the OFR, which has been pointed out in a previous study (Bianchi et al., 2019). The accretion reactions in the OFR are relatively more significant than it should be in the ambient atmosphere. We do not mean to compare HOM monomer and HOM dimer signals crossly here, but to pay attention to their formulae."

(Line 453), which reads,

"of the HOM monomer products (Figure 2a)"

and (Line 577 – 578), which reads,

"and $C_{18}H_{28}O_{10}$ contributed more than 50% of total HOM dimer signals at any OH exposure levels (Figure 2b)."

In addition, we have revised Figure 1 with stacked plots of the distributions of HOM products, and moved the original Figure S2 into the main text as Figure 2b.

(a)

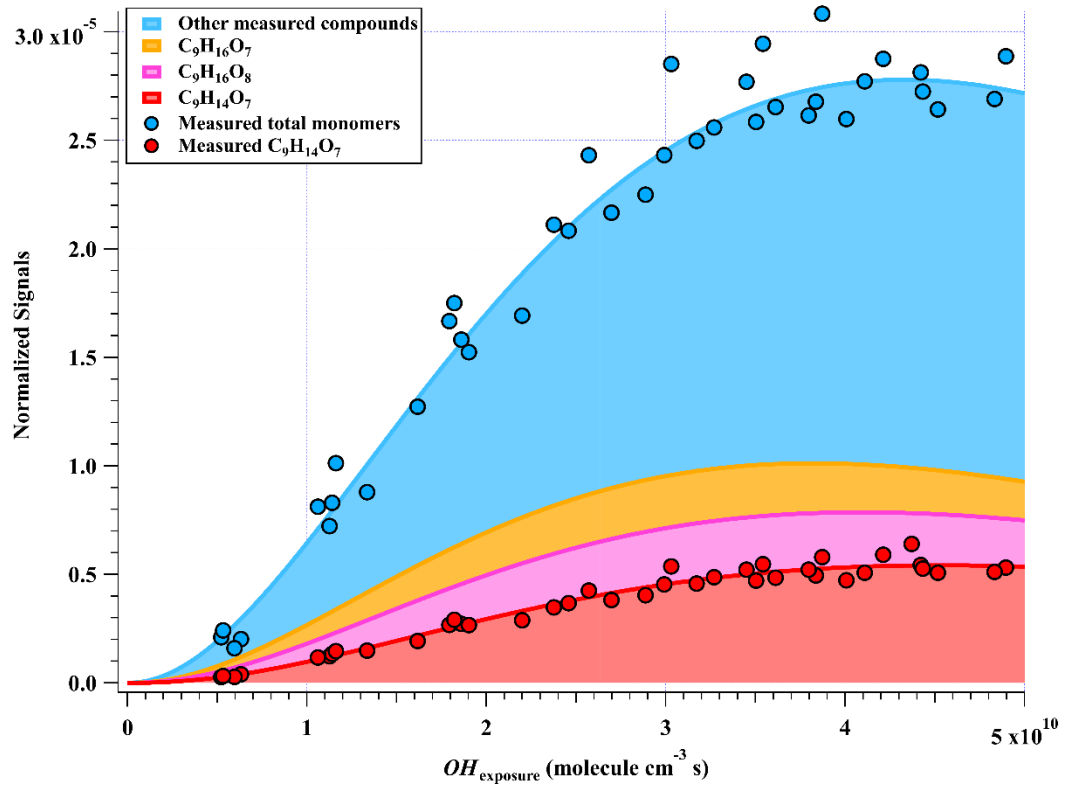

(b)

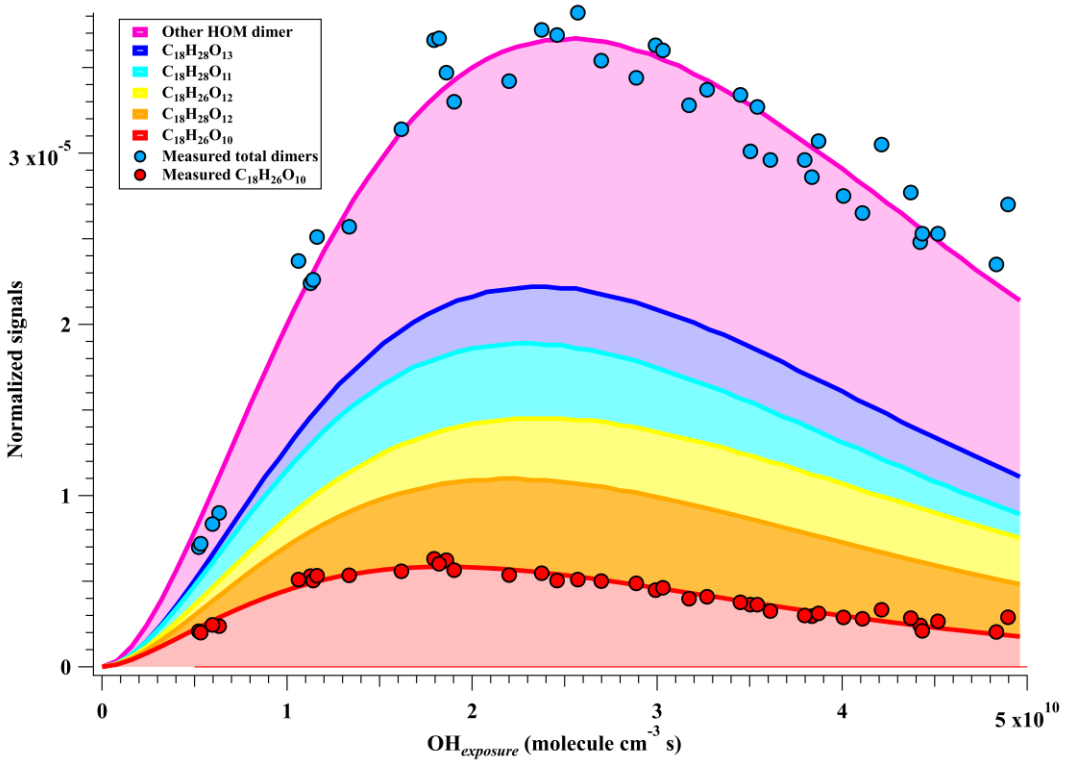

Figure 2. Normalized signals of (a) HOM monomers and (b) HOM dimers versus OH exposure, which are fitted via a gamma function and shown in stacked.

Q 1.11. *"Indeed, laboratory experiments show that RO_2 formed during the second-generation OH oxidation of the first-generation stabilized oxidation products can also undergo autoxidation reactions,"*
→ This is extremely natural, as autoxidation is 'auto-catalytic oxidation' and mainly enabled by the loosening of the adjacent H-atoms next to the gained functional groups. Autoxidation inherently accelerates in many, if not all, chemical systems.

Response 1.11:

Since Reviewer #1 agrees with our argument, nothing has been changed here.

Q 1.12. *"High atmospheric concentrations of OH"*
→ What is high atmospheric concentration to you? In the atmosphere [OH] is mostly buffered by [CO] and [CH4].

Response 1.12:

Thanks for pointing out this vague expression. We have revised our manuscript (Line 121 – 124), which reads,

"OH with an atmospheric concentration up to $6\times10^6 – 2.6\times10^7$ molecule cm^{-3}, which is several times higher than the typical average atmospheric OH concentration, i.e., 1.5×10^6 molecule cm^{-3} (Jacob, 1999), has been frequently observed in both urban and suburban environments in China (Tan et al., 2019; Lu et al., 2012)."

Q 1.13. *Figure S4 has a good idea but is difficult to read with such a small scale.*

Response 1.13:

We have replotted this figure (Figure S3 in the revised supplement), as shown below,

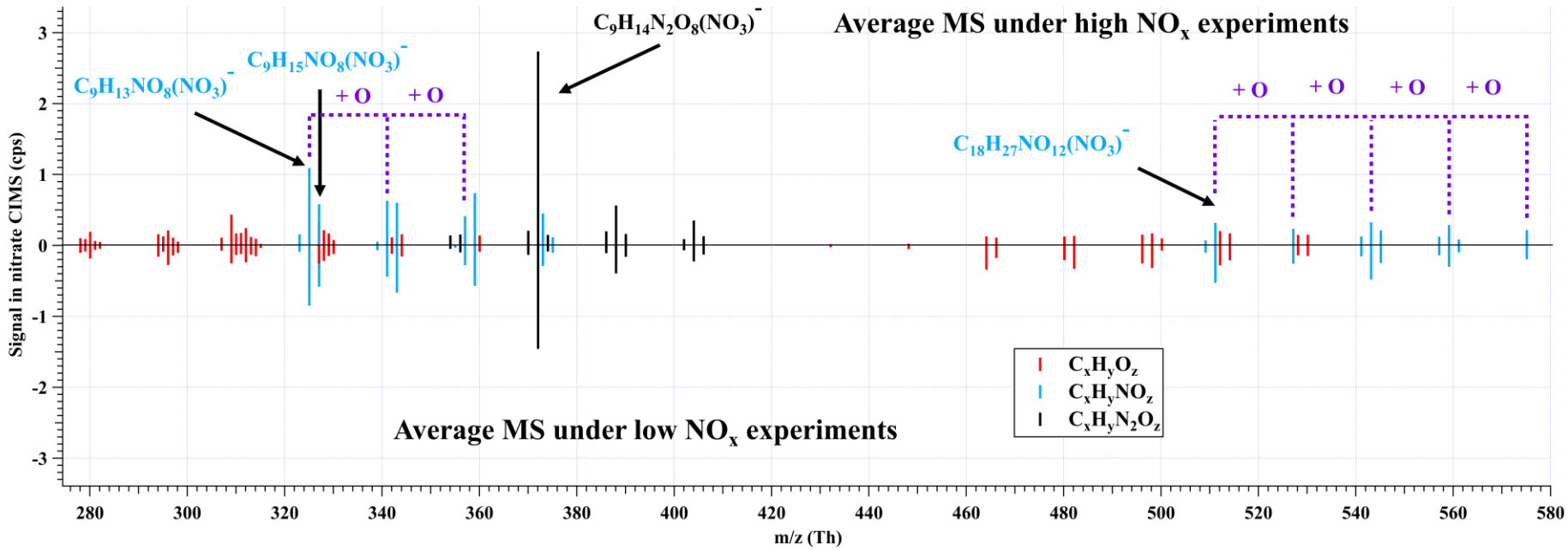

Figure S3. Average mass spectrometry of HOMs detected by nitrate CIMS in the NO_x experiments, presented with the averaged normalized signals in 1.8 ppb NO + 70 ppb NO_2 and 4.8 ppb NO + 120 ppb NO_2 experiments. For comparison, the mass spectrometry under the low NO_x experiments is shown in opposite values.

Q 1.14. *Was the aromatic sample illuminated with the same light source that was used for N_2O photolysis? If so, then the influence of photochemistry is likely important for the results obtained.*

Response 1.14:

In fact, in our experiment settings, N_2O did not photolyze, but reacted with $O(^1D)$ generated via photolysis of O_3 at 254 nm UV light, as stated in the original manuscript (Line 160 – 161). Our setting is different from those in previous studies where N_2O was photolyzed with 185 nm UV light to form $O(^1D)$ and then generate NO (Lambe et al., 2017).

Our settings have been validated in a number of previous investigations (Lambe et al., 2017; Peng and Jimenez, 2020; Lambe et al., 2018). In fact, irradiance of 254 nm in the NO_x experiments was no more than 1.8×10^{15} photons cm^{-2} s. The influence of such a low level of irradiance, i.e., photolysis of the parent aromatics and the first-generation products was not significant, as discussed in Response 1.2.

Q 1.15. *You make a point that estimating HOM penetration through the system to the detector is difficult to quantify, yet it seems your calculations assume that 1,3,5-TMB and HOMs have similar losses in the system. This does not seem reasonable. How does this then influence the determined "nominal relative molar yields of HOMs"?*

Response 1.15:

As shown in Section S1 of the original manuscript, when we estimated the "nominal relative molar yields", the penetration efficiency of HOMs was set as k_{loss}, since the measured signals of HOMs were regarded not as true values at the exit of the OFR, but as values after diffusion loss.

On the other hand, we measured the concentration of 1,3,5-TMB at the exit of OFR by the Vocus-PTR through a sampling line, and regard the measured value as that at the exit of the OFR. Therefore, the loss coefficient of TMB through the system to the detector was assumed to be 0 s^{-1}. We did not assume HOMs and their parent compound have similar losses.

Meanwhile, the concept of "nominal relative molar yields of HOMs" has been removed in the revised manuscript as suggested by Reviewer #2.

Q 1.16. *What do you mean by increase being monotonic or non-monotonic?*

Response 1.16:

A monotonic function is a function that is either entirely nonincreasing or nondecreasing. In other words, a function is monotonic if its first derivative does not change positive/negative signs and does not need be continuous (Royden and Fitzpatrick, 2018). Then, non-monotonic function is a function whose derivative changes positive/negative signs.

According to the gamma function fitting for HOM monomers and dimers, the derivatives of the fitting function of HOM monomers did not change sign during the intraday OH exposure, but the derivatives of HOM dimers did. Thus, we used the terms "increase monotonically or non-monotonically" to describe their behavior.

Q 1.17. *Almost all the monomeric termination products in Scheme 1 have two strong H-bonding*

functional groups (i.e., -OH and -OOH), and thus would be expected to be seen with nitrate ion charging (see, e.g., https://pubs.acs.org/doi/10.1021/acs.jpca.7b10015). Perhaps the proposed scheme is not correct?

Response 1.17:

The proposed scheme is exactly MCM, except for compounds generated after autoxidation.

We double checked the mass spectrometry. Indeed, $C_9H_{12}O_4$, $C_9H_{14}O_4$, and $C_9H_{14}O_5$ were not detected by our nitrate CIMS. Among them, $C_9H_{12}O_4$ and $C_9H_{14}O_4$ were not reported in previous nitrate CIMS measurements, either (Molteni et al., 2018; Tsiligiannis et al., 2019). $C_9H_{14}O_5$ was reported to be detected by nitrate CIMS in previous studies (Molteni et al., 2018; Tsiligiannis et al., 2019), but not shown in our experiments. This phenomena is likely due to the relatively low detection efficiency of compounds with fewer than 5 oxygen atoms by nitrate CIMS, which has been illustrated in previous chamber experiments (Riva et al., 2019).

We have revised our manuscript (Line 448 - 451), which reads,

"The monomeric termination products of BPR, as shown in Scheme 1, were not detected by nitrate CIMS due to their low oxygen contents and thus relative low detection efficiencies in nitrate CIMS, which has been investigated in a previous study (Riva et al., 2019). Those …"

Q 1.18. *"because products from the secondary reactions cannot share the same structure as that of the one from the first-generation reaction."*
→ Except perhaps in recycling or regeneration reactions. However, the important bit here is that you can make isomeric products, and the mass spectrometric detection utilized here would not separate them.

Response 1.18:

Thanks for this excellent point.

We have revised our manuscript (Line 460 - 462), which reads,

"…the one from the first-generation reaction. However, limited by the inherent disadvantages of mass spectrometers, we could not distinguish isomers here and further illustrate their different chemical behaviors."

Q 1.19. *"$C_{18}H_{26}O_8$ can only be formed via the accretion reaction of two $C_9H_{13}O_5$·"*
→ Nope. Could be, for example, through O3 and O7 radicals as well.

Response 1.19:

Only one investigation studied accretion reactions of 1,3,5-TMB-derived BPR, $C_9H_{13}O_5$·, and its autoxidation product, $C_9H_{13}O_7$·, and reported formation mechanisms of $C_{18}H_{26}O_8$ and $C_{18}H_{26}O_{10}$ (Berndt et al., 2018). We propose that $C_{18}H_{26}O_8$ can only be formed via the accretion reaction between two $C_9H_{13}O_5$· in the original manuscript., while Reviewer #1 argued that it might be formed via the accretion reaction between $C_9H_{13}O_3$· and $C_9H_{13}O_7$· based on their formulae.

To our knowledge, $C_9H_{13}O_3$· can only be formed after addition of a hydroxyl radical to the aromatic ring of 1,3,5-TMB and a subsequent O_2 addition to the newly formed hydroxyl-substituted cyclohexadienyl radical (Vereecken, 2019). However, the lifetime of this radical is extremely short, as $C_9H_{13}O_3$· will undertake a ring-closure reaction and get attached by a O_2 very rapidly, forming

the BPR, $C_9H_{13}O_5$· (Vereecken, 2019; Wang et al., 2013, 2017; Li and Wang, 2014). Therefore, $C_9H_{13}O_3$· is not listed as a product of the OH oxidation of 1,3,5-TMB in the MCM (Jenkin et al., 2003; Vereecken, 2019). Indeed, the concentrations of this radical is very low as evidenced by the non-detection of $C_9H_{13}O_3$· in NH_4^+-CI3-TOF measurements in the experiments of Berndt et al. (2018), and are not likely to play an important role in the accretion reactions.

We've revised our manuscript (Line 561 - 567), which reads,

"$C_9H_{13}O_3$· is not likely to react with $C_9H_{13}O_7$· to form large amounts of $C_{18}H_{26}O_8$. $C_9H_{13}O_3$· can only be formed after addition of a hydroxyl radical to the aromatic ring of 1,3,5-TMB and a subsequent O_2 addition to the newly formed hydroxyl-substituted cyclohexadienyl radical (Vereecken, 2019). However, the lifetime of this radical is extremely short, as $C_9H_{13}O_3$· will undertake a ring-closure reaction and get attached by a O_2 very rapidly, forming BPR, $C_9H_{13}O_5$·. Its short lifetime and low concentration, as indicated by Berndt et al. (2018), lead to its insignificant role in the accretion reactions,."

Q 1.20. *I don't understand what the point of the next sentence is: "There are currently no evidences supporting that C9H15Om· radicals can participate in the formation of HOM dimers with 28 hydrogens." Why would you expect the H15 radicals behave in a unique way? But also, supposedly none of the previous studies used as high OH dose, which would explain why such products were not observed. The general observation of dimers with H28 dominating seems worrying.*

Response 1.20:

We acknowledge that there are neither theoretical nor experimental evidences to support a unique behavior of $C_9H_{15}O_m$· radicals. As a result, HOM dimers with 28 hydrogen atoms could also be formed via the accretion of a $C_9H_{13}O_m$· radical and a $C_9H_{15}O_m$· radical. However, since a $C_9H_{15}O_m$· radical, as suggested by its hydrogen atom number, can only be formed via an OH addition to the stabilized $C_9H_{14}O_m$ products through multi-generation OH reactions, our conclusion that $C_{18}H_{28}O_x$ are multi-generation OH oxidation products still holds.

In fact, $C_{18}H_{28}O_x$ have been observed frequently in the OH-initiated oxidation of 1,3,5-TMB at low OH exposures (Molteni et al., 2018; Tsiligiannis et al., 2019), which should not be regarded as a sign of overoxidation.

Firstly, the OH dose in our experiments cannot be considered as high as those in previous laboratory experiments investigating HOMs' generation by OH-initiated oxidation of aromatics (Garmash et al., 2020), as discussed in our Response 1.1.Secondly, OH oxidation experiments of 30 ppb 1,3,5-TMB at a relatively low OH exposure, i.e., 3.5×10^9 molecule cm^{-3} s, show that the total signals of $C_{18}H_{26}O_m$ was close to those of $C_{18}H_{28}O_m$ (Tsiligiannis et al., 2019), representing 8.5% and 7.1%, respectively, of total signals detected by the nitrate CIMS.

Among all the reported experiments that have investigated the distribution of HOMs generated from the OH-initiated oxidation of 1,3,5-TMB (Molteni et al., 2018; Wang et al., 2020; Tsiligiannis et al., 2019), the Molteni et al. (2018) study used the lowest OH dose and precursor concentrations. Nevertheless, $C_{18}H_{28}O_x$ and $C_{18}H_{30}O_x$, in addition to the multigeneration OH product of $C_9H_{16}O_x$, were also detected, which indicate that the oxidation of stabilized products can start at a very early stage.

We've revised our manuscript (Line 584 - 589), which reads,

"In addition, $C_{18}H_{28}O_x$ can also be formed through accretion of a $C_9H_{13}O_m$· radical and a

$C_9H_{15}O_m$· radical, as suggested by previous studies (Molteni et al., 2018; Wang et al., 2020; Tsiligiannis et al., 2019). However, since a $C_9H_{15}O_m$· radical, as suggested by its hydrogen atom number, can only be formed via an OH addition to the stabilized $C_9H_{14}O_m$ products through multi-generation OH reactions, our conclusion that $C_{18}H_{28}O_x$ are multi-generation OH oxidation products still holds. …".

Q 1.21. *It seems worrying that the dimer products decrease already at such a short reaction times. This seems to amply indicate how skewed the chemical system is and that either further chemical processing, or aerosol formation, reduced the dimer yield.*

Response 1.21:

Please refer to our Response 1.1 and 1.10.

The aerosol formation is unlikely to play a role, as particles generated in the PAM OFR were limited.

The exact appearance time of the maximum concentrations of HOM dimers is dependent on the formation rate and loss rate. The formation rate and loss rate were not accelerated equally. On the other hand, the loss pathways of HOM dimers were not exactly the same as the ambient due to the lack of aerosols in the OFR. With the decrease of particulate pollution and thus condensation sinks in the polluted areas, the physical loss of HOMs might be lower and the chemical process can be more important in the ambient.

This series of experiments are not meant to specifically find out the detailed OH exposures when the maximum concentrations of HOM dimers will occur , but try to indicate how HOM dimers evolve with the increase of OH exposures in chemistry. This work can be regarded an indicator for the potential chemical fates of HOM dimers in the atmosphere.

Meanwhile, the concept of "nominal relative molar yields of HOMs" has been removed in the revised manuscript.

We have revised our manuscript (Line 600 - 614) as:

"This decrease of dimer at relatively high OH exposures are likely due to the accelerated accretion reactions in the OFR, resulted by the high RO_2 concentrations. The HOM dimers are formed earlier compared to under ambient conditions and then can go through the further oxidation reactions. Note that this does not mean the maximum concentrations of HOM dimers will also accurately occur at the same OH exposures in the atmosphere, because the detailed appearance time of the maximum concentrations of HOM dimers is dependent on their formation rate and loss rate. In our experiments, the formation rate and loss rate were not accelerated equally. On the other hand, the loss pathways of HOM dimers were not exactly the same as the ambient due to the lack of aerosols in the OFR. With the decrease of particulate pollution and thus condensation sinks in the polluted areas, the physical loss of HOMs might be lower and the chemical process can be more important. This series of experiments are not meant to specifically find out the detailed OH exposures when the maximum concentrations of HOM dimers will occur, but try to indicate how HOM dimers evolve with the increase of OH exposures. This work can be regarded as an indicator for the potential chemical fates of HOM dimers in the atmosphere.

"

Q 1.22. *A OH:HO_2 ratio is given two times although it should presumably be RO_2:HO_2*

Response 1.22:

Sorry for this mistake. We have revised our manuscript (Line 640), which reads,

"Such a high HO_2: RO_2 ratio condition is typically difficult to …"

and Line (642 – 644), which reads,

"This is exactly the case for our experiments, but its influences on our conclusion were tiny, as have been discussed in the Section 3.1."

Q 1.23. *Consider the part: "In addition, high concentrations of radicals might also terminate the RO2 chain earlier, which inhibits the autoxidation reactions in the PAM OFR." This is true. The RO2 lifetime is critically shortened likely inhibiting normally competitive H-shift isomerization reactions. Then consider: "However, these could only influence the distribution of oxidation products at most, and would not affect the chemical behaviors of HOMs under different OH exposures." This is not true. Both conditions favor oxidation of the aromatic parent molecule, but the same HOMs are unlikely to form under so different oxidation conditions.*

Response 1.23:

As stated in our Response 1.1, autoxidation always dominates the fates of RO_2, in both laboratory experiments and ambient atmosphere, because of its rapid reaction rate constant. Meanwhile, because of the similar RO_2 lifetimes between in the laboratory and in the ambient, the RO_2 lifetime is not "critically shortened".

In our experiments either with or without NO_x, the ratios between different radicals were similar to those in the ambient, whilst NO:RO_2 in the laboratory experiments was lower compared to the ambient value, which means that the bimolecular reactions except for RO_2 + NO were accelerated similarly. Nevertheless, the monomeric organonitrates generated in our experiments should have the same formulae as those generated in the ambient though in a lower yield, because their formation pathways were not influenced. The existence of multi-generation OH oxidation can be confirmed via the detection of compounds with multiple nitrogen atoms. On the other hand, compounds generated via $R1$ - $R7$ in the lab will also be generated in the ambient, though their proportions were smaller in the ambient because of the dominant reaction channel of RO_2 + NO ($R8$ - $R9$).

Therefore, differences between the laboratory experiments and the ambient exist, which leads to differences in the distribution of products. However, differences in the distribution of products will not change our conclusion that considerable HOMs can be generated by multi-generation within an intraday OH exposure.

We have revised our manuscript (Line 644 - 648), which reads:

" … in the Section 3.1. Therefore, the difference in the distribution of products will not change our conclusion."

Q 1.24. *"The OH reaction rate for C18H26O8 should be around twice of these values, as there are two*

C=C bonds in its structure. Our calculation result is consistent with this estimation."
→ This seems extremely unlikely as the indicated rate is already basically at the collision limit and the big dimer compound is sterically hindered, which would imply a lower reaction rate.

Response 1.24:

The collision limit at the room temperature is around 9×10^{-10} molecule^{-1} cm^3 s^{-1} (Molteni et al., 2019), which is still much larger than our estimated reaction rate constants. To be rigorous, we now only emphasize on the fast reaction rate constant of $C_{18}H_{26}O_8$ instead of an exact estimation value.

We have revised our manuscript (Line 659 – 660), which reads,

"The OH reaction rate for $C_{18}H_{26}O_8$ should also be fast due to the C=C bonds in its structure, which is activated by the adjacent functionalities."

Q 1.25. *"because the NO termination reaction of RO_2 is the only pathway that can generate organonitrates"*
→ Why would NO_3 or NO_2 chemistry not form organonitrates?

Response 1.25:

We meant to suggest that the NO termination reaction of RO_2 is the only pathway that can efficiently generate organonitrates in our experiments. Organonitrates formed via reactions between NO_2 and RO_2 are believed to be unstable. On the other hand, concentrations of NO_3 were quite low (< 1 pptv estimated by the modified PAM_chem_v8) in our system because of the existence of decent concentrations of NO, which would react with NO_3 at a rapid reaction rate, i.e., 2.7×10^{-11} molecule^{-1} cm^3 s^{-1} (IUPAC dataset, https://iupac-aeris.ipsl.fr, last access: 26 October 2023). Therefore, reactions between NO_3 and RO_2 would not generate organonitrates notably, either.

We've revised our manuscript (Line 533 – 543), which reads,

"…because the NO termination reaction of RO_2 is the only pathway that can generate sufficient amounts of organonitrates in our experiments and …, as indicated in Scheme 2. RO_2 can react with NO_2 to form peroxynitrates ($ROONO_2$) but these species are thermally unstable except at very low temperatures or when the RO_2 is an acylperoxy radical (Orlando and Tyndall, 2012), neither of which were not met in our experiments. The concentrations of NO_3 are estimated to be lower than 1 pptv by our modified PAM_chem_v8 because of the existence of decent concentrations of NO, which would consume NO_3 with a rapid reaction rate constant, i.e., 2.7×10^{-11} molecule^{-1} cm^3 s^{-1} (IUPAC dataset , https://iupac-aeris.ipsl.fr, last access: 26 October 2023). Therefore, NO_2 and NO_3 were unlikely to react with RO_2 to form large amounts of organonitrates in our experiments."

Q 1.26.*A strange comment considering previous literature: "since no evidence supports that a nitrogen-containing monomeric RO2 can go through accretion reactions.*

Response 1.26:

We acknowledge that we could not provide strong evidences for this point. Either a $C_9H_{15}O_m$· radical and a $C_9H_{12}NO_m$· radical, or a $C_9H_{13}O_m$· radical and a $C_9H_{14}NO_m$· radical can react to form a $C_{18}H_{27}NO_m$.

We have revised our manuscript (Line 664 – 668), which reads,

"$C_{18}H_{27}NO_{12}$ can also be formed either by accretion between a $C_9H_{15}O_m$· radical and a $C_9H_{12}NO_m$· radical or accretion between a $C_9H_{13}O_m$· radical and a $C_9H_{14}NO_m$· radical. Both $C_9H_{15}O_m$· and $C_9H_{14}NO_m$· radicals are a typical multi-generation RO_2 and thus prove $C_{18}H_{27}NO_{12}$ is a multi-generation OH oxidation product. Other C18 organonitrates are believed to be formed in a similar pathway. Hence, …" .

References

Assaf, E., Song, B., Tomas, A., Schoemaecker, C., and Fittschen, C.: Rate Constant of the Reaction between CH 3 O 2 Radicals and OH Radicals Revisited , J. Phys. Chem. A, 120, 8923–8932, https://doi.org/10.1021/acs.jpca.6b07704, 2016.

Assaf, E., Tanaka, S., Kajii, Y., Schoemaecker, C., and Fittschen, C.: Rate constants of the reaction of C2–C4 peroxy radicals with OH radicals, Chem. Phys. Lett., 684, 245–249, https://doi.org/10.1016/j.cplett.2017.06.062, 2017.

Berndt, T., Scholz, W., Mentler, B., Fischer, L., Herrmann, H., Kulmala, M., and Hansel, A.: Accretion Product Formation from Self- and Cross-Reactions of RO2 Radicals in the Atmosphere, Angew. Chemie - Int. Ed., 57, 3820–3824, https://doi.org/10.1002/anie.201710989, 2018.

Bianchi, F., Kurtén, T., Riva, M., Mohr, C., Rissanen, M. P., Roldin, P., Berndt, T., Crounse, J. D., Wennberg, P. O., Mentel, T. F., Wildt, J., Junninen, H., Jokinen, T., Kulmala, M., Worsnop, D. R., Thornton, J. A., Donahue, N., Kjaergaard, H. G., and Ehn, M.: Highly Oxygenated Organic Molecules (HOM) from Gas-Phase Autoxidation Involving Peroxy Radicals: A Key Contributor to Atmospheric Aerosol, Chem. Rev., 119, 3472–3509, https://doi.org/10.1021/acs.chemrev.8b00395, 2019.

Bossolasco, A., Faragó, E. P., Schoemaecker, C., and Fittschen, C.: Rate constant of the reaction between CH3O2 and OH radicals, Chem. Phys. Lett., 593, 7–13, https://doi.org/10.1016/j.cplett.2013.12.052, 2014.

Brune, W. H.: The Chamber Wall Index for Gas-Wall Interactions in Atmospheric Environmental Enclosures, Environ. Sci. Technol., 53, 3645–3652, https://doi.org/10.1021/acs.est.8b06260, 2019.

Caravan, R. L., Khan, M. A. H., Zádor, J., Sheps, L., Antonov, I. O., Rotavera, B., Ramasesha, K., Au, K., Chen, M. W., Rösch, D., Osborn, D. L., Fittschen, C., Schoemaecker, C., Duncianu, M., Grira, A., Dusanter, S., Tomas, A., Percival, C. J., Shallcross, D. E., and Taatjes, C. A.: The reaction of hydroxyl and methylperoxy radicals is not a major source of atmospheric methanol, Nat. Commun., 9, 1–9, https://doi.org/10.1038/s41467-018-06716-x, 2018.

Cheng, X., Chen, Q., Li, Y. J., Zheng, Y., Liao, K., and Huang, G.: Highly Oxygenated Organic Molecules Produced by the Oxidation of Benzene and Toluene in a Wide Range of OH Exposure and NOx Conditions, Atmos. Chem. Phys., 1–23, https://doi.org/10.5194/acp-2021-201, 2021.

Crounse, J. D., Nielsen, L. B., Jørgensen, S., Kjaergaard, H. G., and Wennberg, P. O.: Autoxidation of organic compounds in the atmosphere, J. Phys. Chem. Lett., 4, 3513–3520, https://doi.org/10.1021/jz4019207, 2013.

Fittschen, C.: The reaction of peroxy radicals with OH radicals, Chem. Phys. Lett., 725, 102–108, https://doi.org/10.1016/j.cplett.2019.04.002, 2019.

Fuller, E. N., Schettler, P. D., and Giddings, J. C.: A new method for prediction of binary gas-phase diffusion coefficients, Ind. Eng. Chem., 58, 18–27, https://doi.org/10.1021/ie50677a007, 1966.

Garmash, O., Rissanen, M. P., Pullinen, I., Schmitt, S., Kausiala, O., Tillmann, R., Zhao, D., Percival, C., Bannan, T. J., Priestley, M., Hallquist, Å. M., Kleist, E., Kiendler-Scharr, A., Hallquist, M., Berndt, T., McFiggans, G., Wildt, J., Mentel, T. F., and Ehn, M.: Multi-generation OH oxidation as a source for highly oxygenated organic molecules from aromatics, Atmos. Chem. Phys., 20, 515–537, https://doi.org/10.5194/acp-20-515-2020, 2020.

Iyer, S., Kumar, A., Savolainen, A., Barua, S., Daub, C., Pichelstorfer, L., Roldin, P., Garmash, O., Seal, P., Kurtén, T., and Rissanen, M.: Molecular rearrangement of bicyclic peroxy radicals is a key route to aerosol from aromatics, Nat. Commun., 14, 4984, https://doi.org/10.1038/s41467-

023-40675-2, 2023.

Jacob, D. J.: Introduction to atmospheric chemistry, Princeton, 1999.

Jenkin, M. E., Saunders, S. M., Wagner, V., and Pilling, M. J.: Protocol for the development of the Master Chemical Mechanism, MCM v3 (Part B): tropospheric degradation of aromatic volatile organic compounds, Atmos. Chem. Phys., 3, 181–193, https://doi.org/10.5194/acp-3-181-2003, 2003.

Kang, E., Root, M. J., Toohey, D. W., and Brune, W. H.: Introducing the concept of Potential Aerosol Mass (PAM), Atmos. Chem. Phys. Atmos. Chem. Phys., 7, 5727–5744, 2007.

Keller-Rudek, H., Moortgat, G. K., Sander, R., and Sörensen, R.: The MPI-Mainz UV/VIS spectral atlas of gaseous molecules of atmospheric interest, Earth Syst. Sci. Data, 5, 365–373, https://doi.org/10.5194/essd-5-365-2013, 2013.

Knap, H. C. and Jørgensen, S.: Rapid Hydrogen Shift Reactions in Acyl Peroxy Radicals, J. Phys. Chem. A, 121, 1470–1479, https://doi.org/10.1021/acs.jpca.6b12787, 2017.

Lambe, A., Massoli, P., Zhang, X., Canagaratna, M., Nowak, J., Daube, C., Yan, C., Nie, W., Onasch, T., Jayne, J., Kolb, C., Davidovits, P., Worsnop, D., and Brune, W.: Controlled nitric oxide production via O(1D) + N2O reactions for use in oxidation flow reactor studies, Atmos. Meas. Tech., 10, 2283–2298, https://doi.org/10.5194/amt-10-2283-2017, 2017.

Lambe, A., Krechmer, J., Peng, Z., Casar, J., Carrasquillo, A., Raff, J., Jimenez, J., and Worsnop, D.: HO x and NO x production in oxidation flow reactors via photolysis of, 1–22, 2018.

Lambe, A. T., Chhabra, P. S., Onasch, T. B., Brune, W. H., Hunter, J. F., Kroll, J. H., Cummings, M. J., Brogan, J. F., Parmar, Y., Worsnop, D. R., Kolb, C. E., and Davidovits, P.: Effect of oxidant concentration, exposure time, and seed particles on secondary organic aerosol chemical composition and yield, Atmos. Chem. Phys., 15, 3063–3075, https://doi.org/10.5194/acp-15-3063-2015, 2015.

Li, R., Palm, B. B., Ortega, A. M., Hlywiak, J., Hu, W., Peng, Z., Day, D. A., Knote, C., Brune, W. H., De Gouw, J. A., and Jimenez, J. L.: Modeling the radical chemistry in an oxidation flow reactor: Radical formation and recycling, sensitivities, and the OH exposure estimation equation, J. Phys. Chem. A, 119, 4418–4432, https://doi.org/10.1021/jp509534k, 2015.

Li, Y. and Wang, L.: The atmospheric oxidation mechanism of 1,2,4-trimethylbenzene initiated by OH radicals, Phys. Chem. Chem. Phys., 16, 17908, https://doi.org/10.1039/C4CP02027H, 2014.

Lu, K. D., Rohrer, F., Holland, F., Fuchs, H., Bohn, B., Brauers, T., Chang, C. C., Häseler, R., Hu, M., Kita, K., Kondo, Y., Li, X., Lou, S. R., Nehr, S., Shao, M., Zeng, L. M., Wahner, A., Zhang, Y. H., and Hofzumahaus, A.: Observation and modelling of OH and HO2 concentrations in the Pearl River Delta 2006: A missing OH source in a VOC rich atmosphere, Atmos. Chem. Phys., 12, 1541–1569, https://doi.org/10.5194/acp-12-1541-2012, 2012.

McMurry, P. H. and Grosjean, D.: Gas and Aerosol Wall Losses in Teflon Film Smog Chambers, Environ. Sci. Technol., 19, 1176–1182, https://doi.org/10.1021/es00142a006, 1985.

Mehra, A., Wang, Y., E. Krechmer, J., Lambe, A., Majluf, F., A. Morris, M., Priestley, M., J. Bannan, T., J. Bryant, D., L. Pereira, K., F. Hamilton, J., R. Rickard, A., J. Newland, M., Stark, H., Croteau, P., T. Jayne, J., R. Worsnop, D., R. Canagaratna, M., Wang, L., and Coe, H.: Evaluation of the chemical composition of gas- And particle-phase products of aromatic oxidation, Atmos. Chem. Phys., 20, 9783–9803, https://doi.org/10.5194/acp-20-9783-2020, 2020.

Molteni, U., Bianchi, F., Klein, F., Haddad, I. El, Frege, C., Rossi, M. J., Dommen, J., and Baltensperger, U.: Formation of highly oxygenated organic molecules from aromatic compounds,

Atmos. Chem. Phys, 18, 1909–1921, https://doi.org/10.5194/acp-18-1909-2018, 2018.

Müller, J. F., Liu, Z., Nguyen, V. S., Stavrakou, T., Harvey, J. N., and Peeters, J.: The reaction of methyl peroxy and hydroxyl radicals as a major source of atmospheric methanol, Nat. Commun., 7, 1–11, https://doi.org/10.1038/ncomms13213, 2016.

Orlando, J. J. and Tyndall, G. S.: Laboratory studies of organic peroxy radical chemistry: An overview with emphasis on recent issues of atmospheric significance, Chem. Soc. Rev., 41, 6294–6317, https://doi.org/10.1039/c2cs35166h, 2012.

Palm, B. B., Campuzano-Jost, P., Ortega, A. M., Day, D. A., Kaser, L., Jud, W., Karl, T., Hansel, A., Hunter, J. F., Cross, E. S., Kroll, J. H., Peng, Z., Brune, W. H., and Jimenez, J. L.: In situ secondary organic aerosol formation from ambient pine forest air using an oxidation flow reactor, Atmos. Chem. Phys., 16, 2943–2970, https://doi.org/10.5194/acp-16-2943-2016, 2016.

Peng, Z. and Jimenez, J. L.: Radical chemistry in oxidation flow reactors for atmospheric chemistry research, Chem. Soc. Rev., 49, 2570–2616, https://doi.org/10.1039/c9cs00766k, 2020.

Peng, Z., Day, D. A., Ortega, A. M., Palm, B. B., Hu, W., Stark, H., Li, R., Tsigaridis, K., Brune, W. H., and Jimenez, J. L.: Non-OH chemistry in oxidation flow reactors for the study of atmospheric chemistry systematically examined by modeling, Atmos. Chem. Phys., 16, 4283–4305, https://doi.org/10.5194/acp-16-4283-2016, 2016.

Praske, E., Otkjær, R. V., Crounse, J. D., Hethcox, J. C., Stoltz, B. M., Kjaergaard, H. G., and Wennberg, P. O.: Atmospheric autoxidation is increasingly important in urban and suburban North America, Proc. Natl. Acad. Sci. U. S. A., 115, 64–69, https://doi.org/10.1073/pnas.1715540115, 2018.

Riva, M., Rantala, P., Krechmer, J. E., Peräkylä, O., Zhang, Y., Heikkinen, L., Garmash, O., Yan, C., Kulmala, M., Worsnop, D., and Ehn, M.: Evaluating the performance of five different chemical ionization techniques for detecting gaseous oxygenated organic species, Atmos. Meas. Tech, 12, 2403–2421, https://doi.org/10.5194/amt-12-2403-2019, 2019.

Royden, H. L. and Fitzpatrick, P.: Real analysis, Fourth edi., Pearson, New York, NY, 2018.

Slater, E. J., Whalley, L. K., Woodward-Massey, R., Ye, C., Lee, J. D., Squires, F., Hopkins, J. R., Dunmore, R. E., Shaw, M., Hamilton, J. F., Lewis, A. C., Crilley, L. R., Kramer, L., Bloss, W., Vu, T., Sun, Y., Xu, W., Yue, S., Ren, L., Acton, W. J. F., Hewitt, C. N., Wang, X., Fu, P., and Heard, D. E.: Elevated levels of OH observed in haze events during wintertime in central Beijing, Atmos. Chem. Phys., 20, 14847–14871, https://doi.org/10.5194/acp-20-14847-2020, 2020.

Tan, Z., Rohrer, F., Lu, K., Ma, X., Bohn, B., Broch, S., Dong, H., Fuchs, H., Gkatzelis, G. I., Hofzumahaus, A., Holland, F., Li, X., Liu, Y., Liu, Y., Novelli, A., Shao, M., Wang, H., Wu, Y., Zeng, L., Hu, M., Kiendler-Scharr, A., Wahner, A., and Zhang, Y.: Wintertime photochemistry in Beijing: Observations of ROx radical concentrations in the North China Plain during the BEST-ONE campaign, Atmos. Chem. Phys., https://doi.org/10.5194/acp-18-12391-2018, 2018.

Tan, Z., Lu, K., Jiang, M., Su, R., Wang, H., Lou, S., Fu, Q., Zhai, C., Tan, Q., Yue, D., Chen, D., Wang, Z., Xie, S., Zeng, L., and Zhang, Y.: Daytime atmospheric oxidation capacity in four Chinese megacities during the photochemically polluted season: A case study based on box model simulation, Atmos. Chem. Phys., 19, 3493–3513, https://doi.org/10.5194/acp-19-3493-2019, 2019.

Tsiligiannis, E., Hammes, J., Salvador, C. M., Mentel, T. F., and Hallquist, M.: Effect of NOx on 1,3,5-trimethylbenzene (TMB) oxidation product distribution and particle formation, Atmos. Chem. Phys., 19, 15073–15086, https://doi.org/10.5194/acp-19-15073-2019, 2019.

Vereecken, L.: Reaction Mechanisms for the Atmospheric Oxidation of Monocyclic Aromatic Compounds, Adv. Atmos. Chem., 377–527, https://doi.org/10.1142/9789813271838_0006, 2019.

Wang, L., Wu, R., and Xu, C.: Atmospheric oxidation mechanism of benzene. Fates of alkoxy radical intermediates and revised mechanism, J. Phys. Chem. A, 117, 14163–14168, https://doi.org/10.1021/jp4101762, 2013.

Wang, S., Wu, R., Berndt, T., Ehn, M., and Wang, L.: Formation of Highly Oxidized Radicals and Multifunctional Products from the Atmospheric Oxidation of Alkylbenzenes, Environ. Sci. Technol., 51, 8442–8449, https://doi.org/10.1021/acs.est.7b02374, 2017.

Wang, Y., Mehra, A., Krechmer, J. E., Yang, G., Hu, X., Lu, Y., Lambe, A., Canagaratna, M., Chen, J., Worsnop, D., Coe, H., and Wang, L.: Oxygenated products formed from OH-initiated reactions of trimethylbenzene: autoxidation and accretion, Atmos. Chem. Phys., 20, 9563–9579, https://doi.org/10.5194/acp-20-9563-2020, 2020.

Xu, L., Møller, K. H., Crounse, J. D., Kjaergaard, H. G., and Wennberg, P. O.: New insights into the radical chemistry and product distribution in the OH-initiated oxidation of benzene, Environ. Sci. Technol., 54, 13467–13477, https://doi.org/10.1021/acs.est.0c04780, 2020.

Yan, C., Kocevska, S., and Krasnoperov, L. N.: Kinetics of the Reaction of CH3O2 Radicals with OH Studied over the 292-526 K Temperature Range, J. Phys. Chem. A, 120, 6111–6121, https://doi.org/10.1021/acs.jpca.6b04213, 2016.